Energy Conversion and Management: X 22 (2024) 100559

Contents lists available at ScienceDirect

Energy Conversion and Management: X

journal homepage: www.sciencedirect.com/journal/energy-conversion-and-management-x

Optimization of power take-off system settings and regional site selection procedure for a wave energy converter

Hossein Mehdipour [a], Erfan Amini [b], Seyed Taghi (Omid) Naeeni [a], Mehdi Neshat [c,d], Amir H. Gandomi [d,e,*]

[a] School of Civil Engineering, College of Engineering, University of Tehran, Tehran 14179, Iran
[b] Department of Civil, Environmental and Ocean Engineering, Stevens Institute of Technology, Hoboken, NJ 07030, United States
[c] Center for Artificial Intelligence Research and Optimization, Torrens University Australia, Brisbane, QLD 4006, Australia
[d] Faculty of Engineering & Information Technology, University of Technology Sydney, Ultimo, NSW 2007, Australia
[e] University Research and Innovation Center, Obuda University, 1034 Budapest, Hungary

ARTICLE INFO

Keywords:
Ocean renewable energy
Oscillating surge wave energy converter
Power take-off optimization
Site selection
Meta-heuristic
Swarm intelligence algorithms

ABSTRACT

Ocean wave energy stands as a crucial component in the quest for sustainable and renewable energy sources, essential in the global effort to mitigate climate change. However, a significant challenge in this field is optimizing the efficiency of Wave Energy Converters (WECs) on a regional scale, particularly Oscillating Surge Wave Energy Converters (OSWECs). This challenge stems from the complex, nonlinear interactions between ocean waves and these devices, necessitating precise tuning of Power Take-Off (PTO) system settings and optimal placement for the highest possible performance and stability. To address this challenge, our study introduces the Hill Climb - Explorative Grey Wolf Optimizer (HC-EGWO), a novel algorithm combining local search and swarm-based global optimization strategies. This hybrid approach effectively balances exploration and exploitation in the solution space, leading to more optimal PTO settings for OSWECs. Alongside this algorithmic development, we conduct a thorough feasibility analysis based on the constraints of the flap's maximum angular motion. This ensures the optimized OSWEC operates within safe and efficient limits. In a comparative analysis with the Genetic Algorithm (GA), the Particle Swarm Optimization (PSO), the artificial Gorilla Troops Optimizer (GTO), and different implementations of the GWO, our results show an improvement in power output, with the HC-EGWO method achieving up to a 3.31% increase over other variations of the GWO and 45% increase compared to all the methods. The findings of this study not only demonstrate the effectiveness of the HC-EGWO method but also provide strategic insights for the deployment of OSWECs in areas like the South Caspian Sea, where unique environmental factors imply careful consideration in the site selection process.

1. Introduction

The importance of ocean renewable energy cannot be overstated, as it offers a promising means to diversify the global energy portfolio, reduce dependence on fossil fuels, and mitigate the impacts of climate change [1]. Due to the vastness and untapped potential of the world's oceans, harnessing their power for sustainable electricity generation is critical for meeting the rising energy demands of an ever-growing global population. Even statistical approaches have been devised to predict the wave power of the ocean [2]. Furthermore, ocean energy resources such as tidal, wave, and Ocean Thermal Energy Conversion (OTEC) exhibit lower variability and higher predictability compared to other renewable sources like wind and solar [3]. However, the ocean wave energy sector has witnessed the most substantial advancements in recent years, with numerous ocean Wave Energy Converters (WECs) under development and testing [4,5]. These devices capture and transform kinetic and potential energy present in ocean waves into electricity [6].

There are several methods for WEC classification. The first one is based on location. The WEC can be located at the shoreline or offshore. Offshore devices can harvest greater amounts of energy. The following criterion is how the device operates; it can be divided into submerged pressure differential, oscillating water column (OWC) [7,8],

* Corresponding author at: Faculty of Engineering and Information Technology, University of Technology Sydney, Ultimo, Sydney 2007, NSW, Australia.
E-mail addresses: hossein.mehdipour@ut.ac.ir (H. Mehdipour), eamini@stevens.edu (E. Amini), stnaeeni@ut.ac.ir (S.T.(O. Naeeni), mehdi.neshat@torrens.edu.au, mehdi.neshat@uts.edu.au (M. Neshat), gandomi@uts.edu.au (A.H. Gandomi).

https://doi.org/10.1016/j.ecmx.2024.100559

Available online 7 March 2024

overtopping device, or oscillating surge wave energy converter [9], which is the most popular one [10]. There are also other types of converters like point absorbers [11], Buoy-Rope-Drum (BRD) WEC [12], and a piezoelectric wave energy harvester [13]. In this research, an offshore OSWEC device is investigated.

The vigorous surge motion, cost-effective installation, and minimal environmental impact have made OSWECs a preferable choice[14]. Numerous studies have investigated the potential of Oscillating Surge Wave Energy Converters (OSWECs) as a viable wave energy conversion technology; for instance, Ghasemipour et al. inspected nearshore regions of the southern coast of Iran for the feasibility of such devices [15]. Folley *et al.* have studied the effects of water depth [16] and device width [17] on the performance of OSWECs. The effects of the device's flap's width [18], length [19], orientation [20], shape, weight, and thickness [21] on the converter's performance have also been studied. It's been shown that the increase in the OSWEC's PTO has positive effects on power and flap's motion amplitude up to a certain point [22]. The wave characteristics like frequency [17] and period [23] can also influence the OSWEC's performance. Moreover, Lin *et al.* showed that, on average, the viscous loss of the fluid decreases the capture factor by 20% [24].

Almost all the numerical simulations in recent years have been based on Computational Fluid Dynamics (CFD). On one end of the spectrum of these methods is the Linear Potential Flow theory models [25], which are fast but not very accurate. On the other hand, some studies [26,27] have used Reynolds Averaged Navier–Stokes Equations (RANS) CFD solvers for WEC analysis and simulation, which are computationally complex and slow but offer higher fidelity [28]. OpenFOAM, an open-source CFD software, has also been used to analyze the effectiveness of energy-maximizing control systems and the Numerical Wave Tanks (NWTs) for WECs [29,30]. MATLAB is another software that has been utilized in this field [31].

Recently, the WEC-Sim module [32], designed for MATLAB and LPF-based, has been extensively used for WEC simulations [33]. Different types of converters like point absorbers [34], OSWECs [35–37], FOSWECs [38–40], and even novel WEC types [41] have been inspected using WEC-Sim. WEC-Sim is an open-source simulation tool designed for WEC numerical simulations [32]. Much research has been utilizing WEC-Sim to investigate OSWEC performance, which encompasses a variety of objectives, for instance, minimizing cost [35], reducing the hydrodynamic loads [42], lowering the applied loads to the support structure of the device [36], and mitigating the horizontal motion of the OSWEC's platform which in turn reduces costs [40].

One of the important aspects of WEC performance improvement is the PTO optimization [43]. In the early studies, the predominant focus of numerical studies was on linear PTOs. For instance, Sheng et al. have optimized two models of linear PTOs for a Wave-Activated Bodies WEC [44] and an OWC [45]. However, researchers have since shown interest in the performance analysis of WECs with a Hydraulic PTO [46,47] or a mechanical one [48]. A variety of optimization studies have also been used in this field. In [49], an improved version of the differential evolution (DE) algorithm was used for a WEC array, simultaneously achieving more precise convergence and speed. Gomes *et al.* [50] did a hull optimization of a floating OWC using DE and COBYLA, a direct search method, to achieve maximum power output. The Genetic Algorithm (GA) has been used widely in the field of wave energy generation; for instance, in [51], it has been used for shape optimization of a planar pressure differential WEC, and in [52,53], the WEC array configuration was optimized as well.

In [54], multiple meta-heuristic optimization algorithms, like GA or Particle Swarm Optimization (PSO), were used for the geometry optimization of WECs. The PSO has also been used for the optimization of WEC systems [55,56]. Furthermore, Neshat et al. devised the improved Moth-Flame Optimizer (MFO) to optimize the geometry and the PTO settings of a generic multi-mode WEC [57]. In [58], the geometry of the wells turbine was improved using an automated optimization technique. Moreover, other meta-heuristic approaches, like the Mulit-Verse Optimizer (MVO) [59], and the Grey Wolf Optimizer (GWO) [6] has been utilized for optimization in the field of other sources of renewable energy as well [60]. Additionally, artificial intelligence methods have been extensively used in this field as well [61,62].

In another study [63], the authors devised an innovative hybrid approach mixing specific fast local search (details can be found in[64]), numerical and evolutionary optimization for a WEC array, enabling them to achieve better solutions faster. In [65], an HPTO of a point absorber was optimized using ten different optimization algorithms. Results showed that a modified combination of Genetic, Surrogate, and fminsearch algorithms outperform others.

Different studies have investigated the potential of wave energy harvesting in the Caspian Sea. Kamranzad et al. [66] found this sea a good location for wave energy exploitation due to its stability in mean wave power during different years. Alamian et al. [67] identified the point absorber device to be the most suitable WEC in this area based on wave and coastal parameters. Amirnia et al. [68] reported a 7.3% loss in exploitable wave energy due to uncertainty considerations.

Multiple studies have found the Mazandaran shore the most suitable location for wave energy harvesting [69], these studies have used different softwares like WEC-Sim [70] and MIKE [71]. Finally, a recent study [72] introduced a centipede WEC and analyzed its performance using Simcenter Amesim software based on the hydraulic PTO parameters in a wave tank.

Extensive studies have been conducted to identify the optimal location for wave energy projects. Iuppa et al. [73] found the best location for a wave energy device by analyzing the wave and wind propagation data based on the energy potential and coast proximity of the potential locations. In [74], a more comprehensive study was done by factoring in environmental (designated marine protected areas) and socio-economical (traditional fishing zones) as well. Ergul et al. [75] suggested a two-step multi-criteria decision-making (MCDM) that first found the best location and then the most suitable WEC for achieving maximum power output.

Kamranzad et al. [76] developed a Multi-Criteria Approach (MCA) to find the best combinations of location/WEC. Then in [77], they modified their method to take into account the wave climate in a 55-year period in China. There has been a MATLAB-based application specifically to estimate the wave energy of a marine area in Spain [78]. Xu et al. [79] proposed a new "top-down" method involving device-agnostic performance constraints and economical factors to find the best location for WEC installation on the West Coast of Vancouver Island. Wang et al. [80] introduced a novel MCDM approach that combines seven methods, including Data Envelopment Analysis (DEA) approach, Fuzzy Best-Worst Method (Fuzzy BWM), etc., to create an integration framework to find the best locations for wave energy harvesting in Australia.

This study proposes a fast and effective hybrid optimization method for maximizing the power absorption of an OSWEC based on the hindcast wave data from nine zones in the Caspian Sea, each has 9–12 data points. The significant contributions of this work are as follows:

- Proposing a novel optimizer to maximize the power absorption of an OSWEC, the Hill Climb-Explorative Gray Wolf Optimizer (HC-EGWO) methodology combines a local search method with a global optimizer to balance exploration and exploitation rates for improved solution quality.
- Developing a technical feasibility landscape analysis utilizing the Wave Energy Converter Simulator (WEC-Sim) numerical model to account for the maximum feasible angular motion of the flap, ensuring optimized OSWEC operation within safety and efficiency limits.
- Insights for selecting optimal offshore sites, optimizing power output, and promoting the adoption of ocean renewable energy sources.

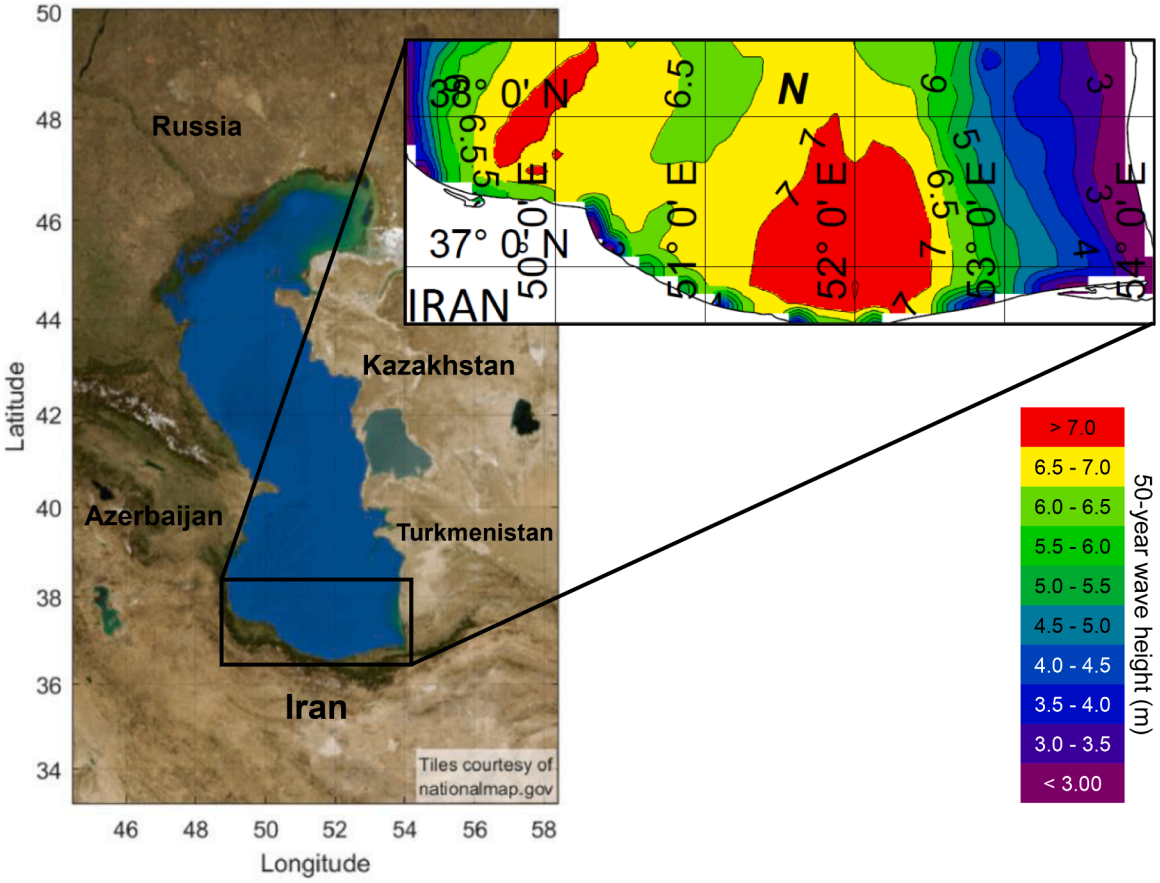

Fig. 1. Projection of 50-year wave height (m) spatial variation in the southern coasts of the Caspian Sea [82,81].

- Achieving a significant increase in power output (up to 58%) compared to other methods demonstrates the effectiveness of the proposed HC-EGWO optimization approach.
- Gaining valuable knowledge for deploying OSWECs in the South Caspian Sea, considering its unique environmental conditions and energy potential.

This study is organized as follows. Section 2 presents the data collection, WEC's feasibility, and other preliminary analyses. Section 3 goes over the multiple modifications of GWO and proposes a new optimization algorithm. The following section provides the benchmark functions used to evaluate the new algorithm's performance. Section 5 presents the problem formulation information. Finally, Section 6 provides the results of the study.

2. Case study landscape analysis

In this study, we selected potential wave energy conversion sites in the Caspian Sea by analyzing wave height and period data. Our approach is grounded in a comprehensive review of existing literature to identify and benchmark against similar works, ensuring our research is both novel and relevant. We then focus on the power take-off optimization of flap-based wave energy converters tailored for the identified hotspots to maximize power production. Recognizing the importance of empirical validation, we outline a future direction for integrating field trials, which are crucial for comparing numerical predictions with real-world data.

2.1. The Caspian Sea

The Caspian Sea is between Iran to the south, Russia to the north, Russia and Azerbaijan to the west, and Turkmenistan and Kazakhstan to the east. This body of water is often categorized either as the largest lake in the world or the most miniature sea on Earth, and it holds the distinction of being the largest landlocked body of water. It spans approximately 1030–1200 km in length and 196–435 km in width. The surface of the Caspian Sea lies around 28 meters below sea level. The northern part of the sea is notably shallow, with only a negligible portion of seawater present in the northern quarter and an average depth of less than 5 meters [81]. Hence, investigating the southern shores becomes more significant for wave analysis. Due to its status as one of Asia's most crucial energy sources, the Caspian Sea has always attracted considerable attention from the industry. The expansion of its southern coast also presents significant potential for harnessing wave energy [70].

Various analyses have been conducted to forecast waves in the southern areas of the Caspian Sea, considering the prevailing direction of the dominant sea waves. Fig. 1 displays the projected values of 50-year dominant waves in the southern regions, utilizing the Gumble distribution [82]. Given the wave heights depicted in Fig. 1, it becomes crucial to identify a point with maximum wave energy that also offers convenient beach access. Therefore, comprehensive research is needed to analyze wave data in the southern Caspian Sea, aiming to identify this point and establish a general criterion for comparing energy levels among different points using parameters such as wave height and wave period.

2.2. Data collection

To investigate the southern coasts of the Caspian Sea, the initial step involved analyzing the data obtained from the Iranian National Institute for Oceanography and Atmospheric Science (INIO). Specifically, the

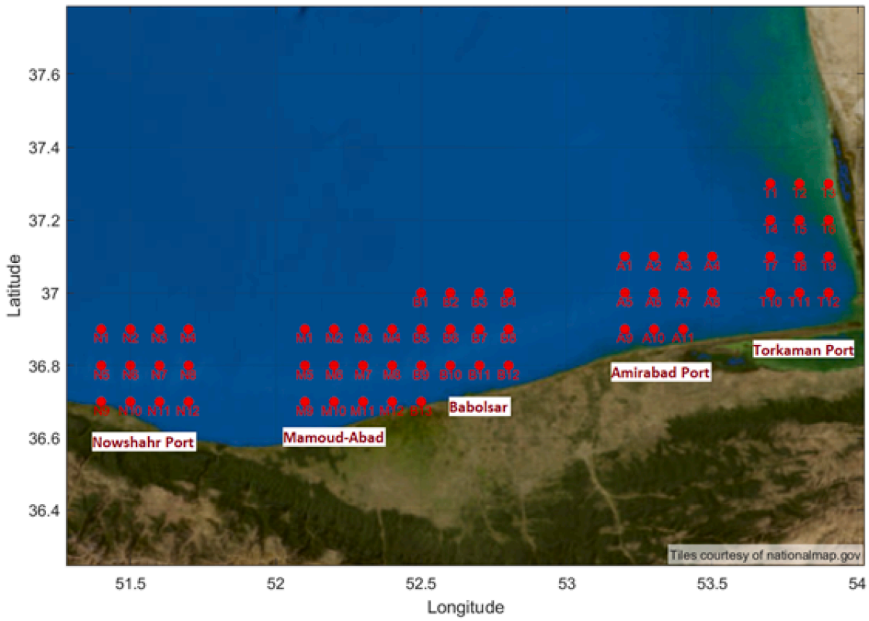

Fig. 2. A representation of the surveyed areas along the southeastern coast of the Caspian Sea, including Torkaman, Amirabad, Babolsar, Mahmoud-Abad, and Nowshahr Port.

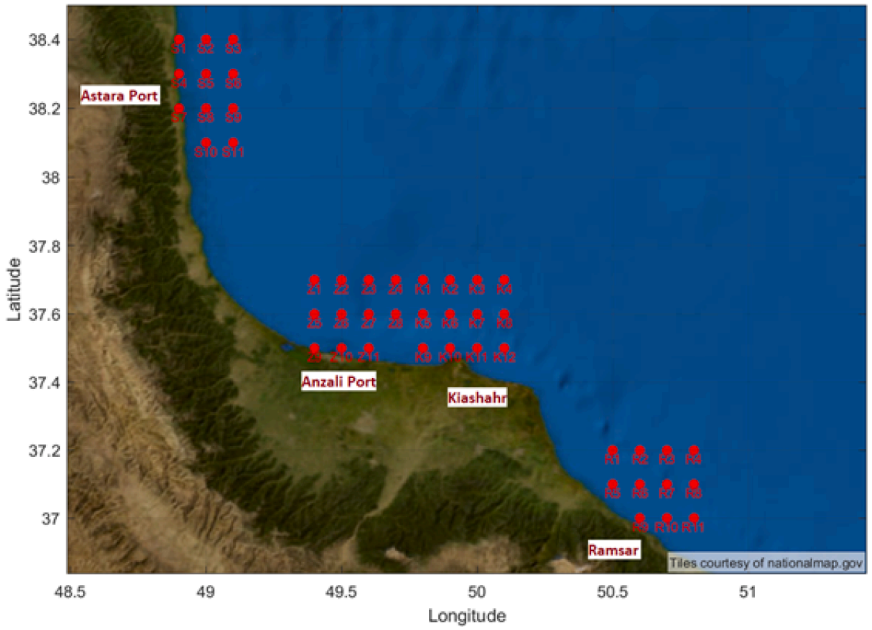

Fig. 3. A representation of the surveyed areas along the southeastern coast of the Caspian Sea, including Ramsar, Kiashahr, Anzali Port, and Astara Port.

applied data from the Iranian Seas Wave Modeling (ISWM) and the Iranian Wave Atlas (IWA) models were examined. These datasets covered the entire Caspian Sea over a five-year period, from January 2006 to December 2010, with 1-h time intervals. With reference to relevant literature and local assessments, nine ports were selected on the southern coasts of the Caspian Sea. A designated area of 0.2 longitude and latitude was considered around these ports, and locations with available data within this area were extracted. In total, 105 data points from the southern coast area of the Caspian Sea were identified, and their specifications are detailed in Fig. 2 and Fig. 3.

2.3. Preliminary analysis

In order to understand the waves in the Caspian Sea, the data from nine selected ports were visualized. This was done by plotting wave rose diagrams (Fig. 4) and wave scatter diagrams (Fig. 5)) to visualize the distribution of wave directions and to identify the prevailing wave patterns in the region. The variations in wave height and wave period across different locations in the study area were unveiled by analyzing the wave scatter diagrams. As seen in Fig. 4, the waves have a relatively small magnitude and are mainly to the north, which is logical because these ports are in the southern part of the Caspian Sea. Moreover, from the scatter wave diagram in Fig. 5, the waves comparably have low heights and low periods, and the most prevalent waves have a height of 20 cm and a period of 3 s.

A power matrix was also made specifically for the Caspian Sea, shown in Fig. 6. This matrix comprehensively assessed the wave energy potential in these regions. It takes into account important factors such as

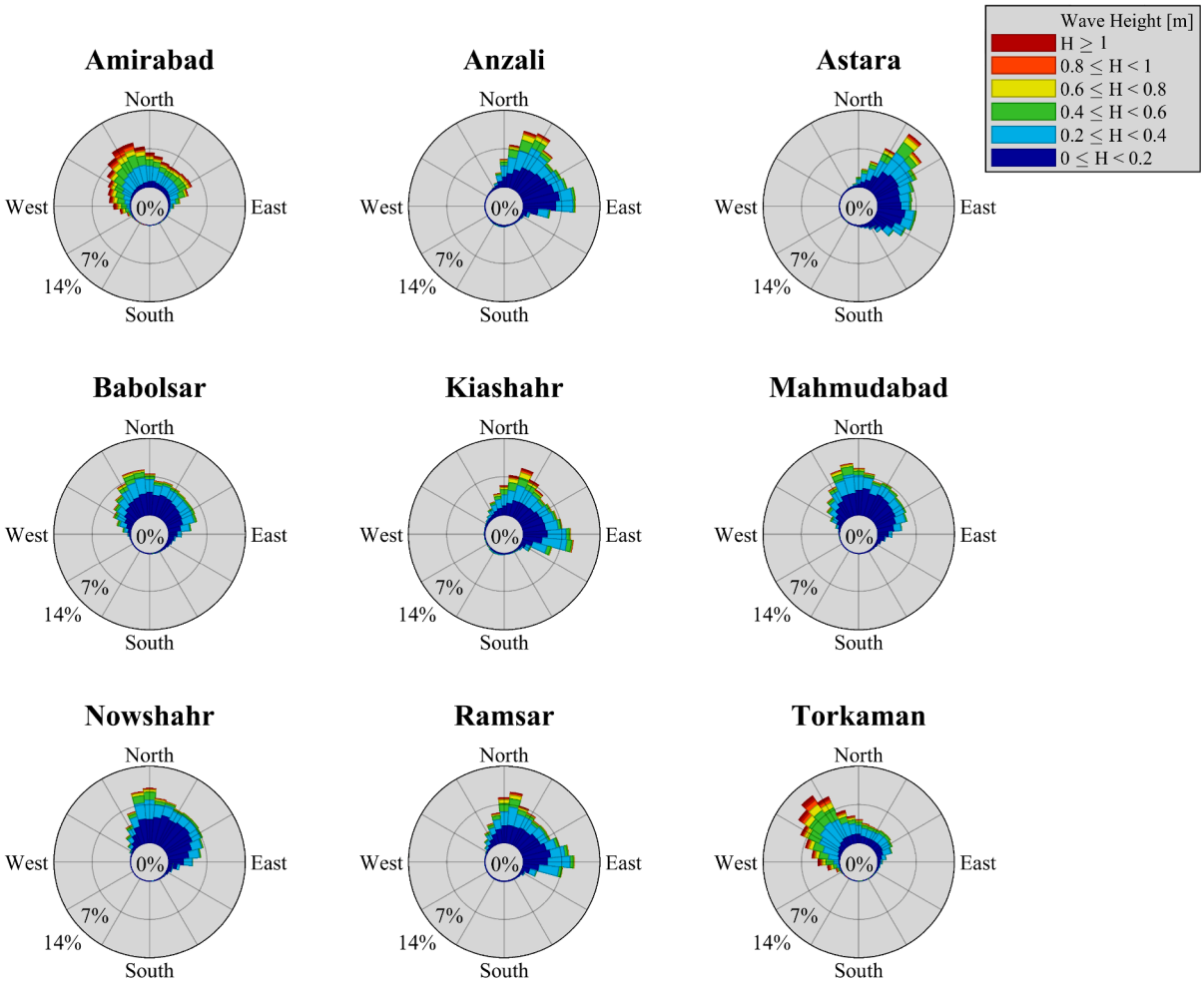

Fig. 4. the wave rose diagram for the nine analyzed sea ports reveals relatively small wave magnitudes that predominantly originate from the north. This observation aligns with expectations since these ports are located in the southern region of the Caspian Sea.

wave height and wave period to estimate the energy conversion capabilities of OSWECs in these areas. As shown in Fig. 6, increasing either the height or the period of the wave can lead to higher absorbed energy.

Collectively, the insights gained from the wave rose diagrams, wave scatter diagrams, and power matrix contribute to our understanding of the spatial distribution of wave energy in the Caspian Sea.

2.4. WEC's feasibility

Analysis of OSWEC's flap interaction with the wave under linear water wave theory assumptions requires the flap's excursions to be adequately small. The reason is that the flap's rotation should be small enough so that the correct and non-linear form of the hydrostatic stiffness, which is $(K_p \sin\theta)$, can be replaced by (K_p) [83]. Several studies [84,23,85,22] assumed the maximum angular motion of the flap to be 30 °) [84]. In addition, this limitation helps the device to avoid damages, particularly in extreme sea states [85]. In Fig. 7, the feasible area of the damping and stiffness of the PTO are presented. First, the literature for the range of viable damping and stiffness values for the PTO was reviewed, the result of which is shown by the orange color. Next, based on the OSWEC's flap oscillation limitation, the feasible values of K_{PTO} and C_{PTO} were finalized, and the red area was omitted. Finally, the remaining area, shown by the color green, represents the applicable range of these two critical parameters.

2.5. Preliminary sensitivity analysis

In order to investigate the impact of critical parameters on the performance of an oscillating wave energy converter, a sensitivity analysis was conducted. Wave height (H), wave period (T), PTO's damping (C), and stiffness (K) were analyzed regarding the power output of the system through six plots in Fig. 8. By examining the plots, valuable insights were obtained regarding the optimal values for these parameters and their combinations for maximizing power generation.

Fig. 8-(a) represents the effect of H and T in optimizing the generated power of the OSWEC. The plot reveals that a combination of high wave height and wave period leads to the best power outputs. However, it is noteworthy that extreme values of T can decrease the power. Fig. 8-(b) illustrates the influence of K and H on the converter's power generation. As can be seen, both high and low levels of PTO stiffness can result in passable power outputs. However, the highest power is achieved when K is moderate. Fig. 8-(c) depicts the relation between C and H and the device's generated power. High wave heights and low values of PTO damping correspond to favourable power outputs and improved performance.

Fig. 8-(d) shows the effects of K and T variation on power. Accordingly, the wave periods within the range of approximately 6 to 9 s yield pleasing power outputs. Furthermore, the power improves significantly as the PTO stiffness approaches its medium values. Fig. 8-(e) showcases the influence of C and T. Similar to the previous plot, wave periods ranging from approximately 6 to 9 s produce the most favourable power outputs—additionally, the performance improves as the PTO damping

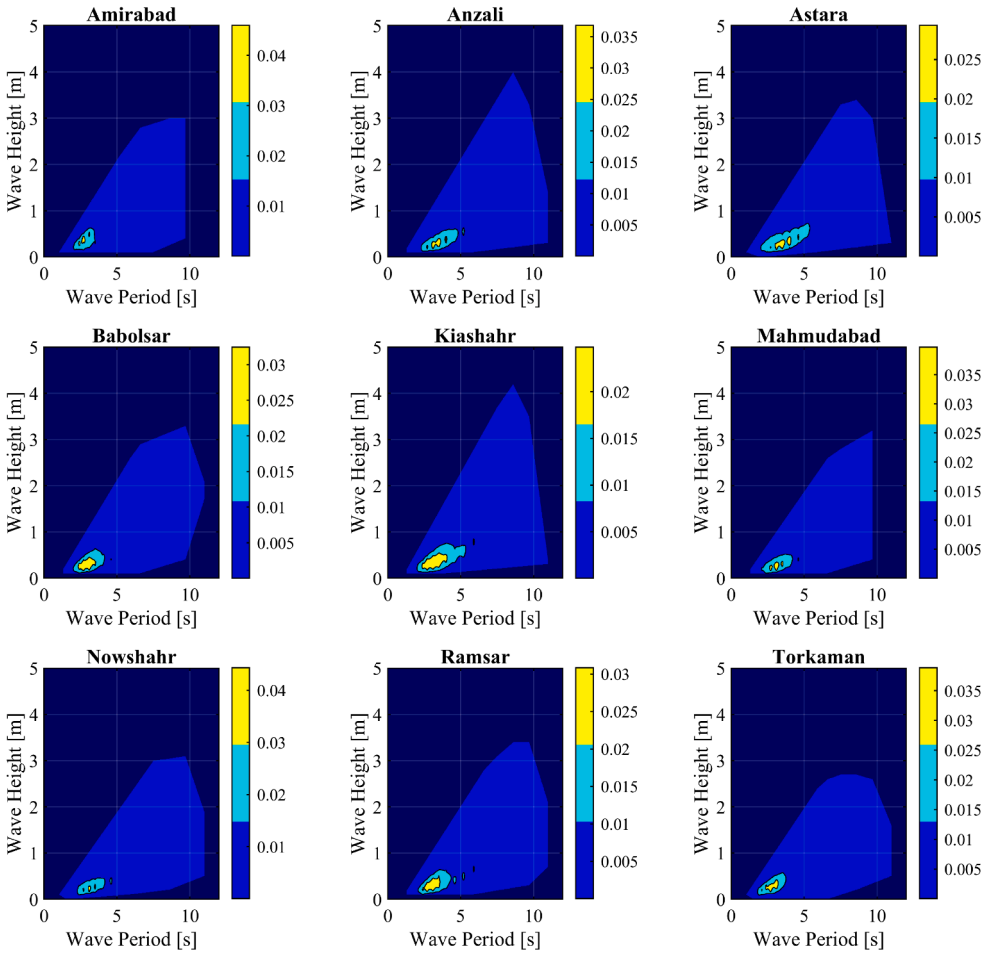

Fig. 5. The wave scatter diagram of the nine studied ports.

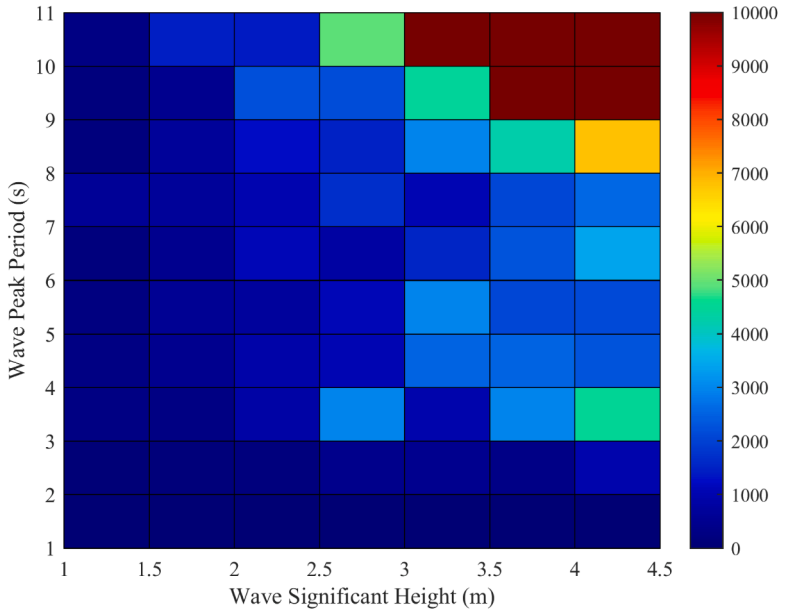

Fig. 6. The power matrix of the southern coasts of the Caspian Sea.

decreases. Finally, in Fig. 8-(f), the PTO parameters regarding their effect on the power output have been investigated. According to the plot, almost always lower values C result in better power, and a K value between 10 and 70 MNm/rad leads to the best performance. Overall, the parameter's effects can be explained relatively simply. In summary, higher H and lower C lead to the best power outputs. Furthermore,

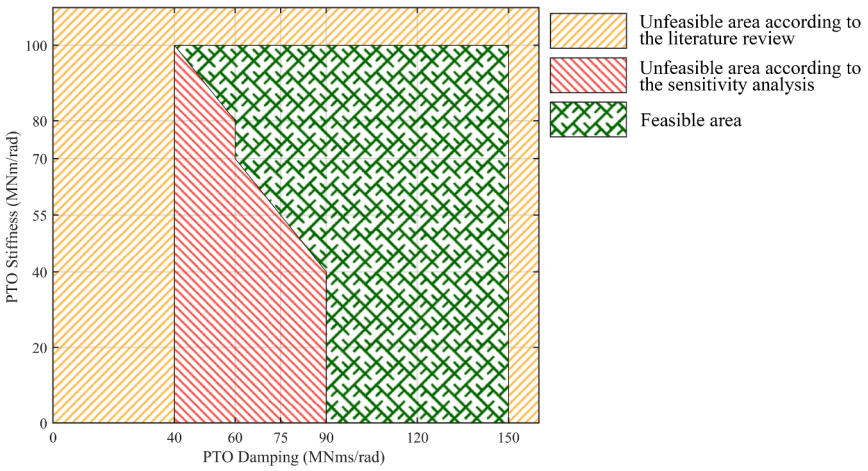

Fig. 7. The feasible area of the PTO damping and stiffness used in this study.

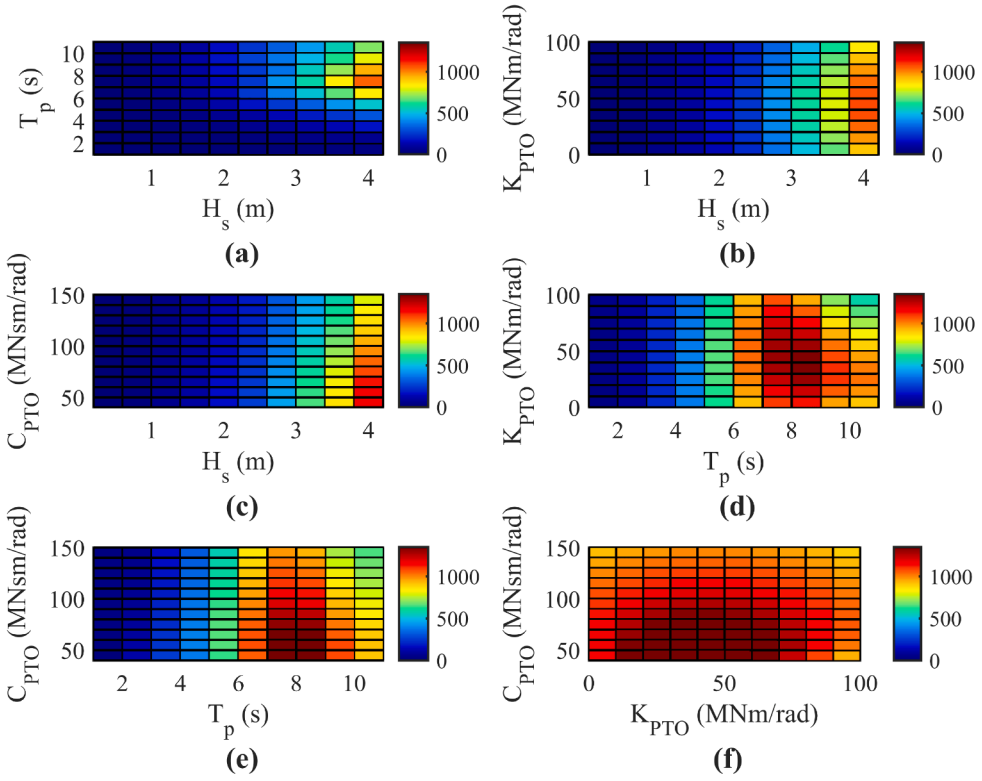

Fig. 8. Sensitivity analysis plots for the key parameters of the OSWEC (Wave height, wave period, PTO damping, and PTO stiffness).

moderate values of T and K lead to the best performance. Overall, it can be seen that the problem at hand is a multimodal optimization problem and has multiple optima.

Next, the effects of the PTO parameters on the PTO power were further inspected in Fig. 9. The black parts show the unfeasible areas calculated in previous sections. Similar to the power output, low values of C and moderate K values bring about the highest PTO forces. It is worth noting that in the OSWEC, the power output is calculated by multiplying PTO force by the flap's velocity [23].

3. Optimization approach

3.1. Genetic algorithm

Genetic Algorithm (GA) is based on the theory of evolution. In this method, each chromosome represents a solution. In each iteration, high-performing chromosomes reproduce to obtain better chromosomes in the next generation. GA does this by utilizing a few mechanisms: selection, crossover, mutation, and elitism. These operations have to be fine-tuned in order to get the best results [86].

Selecting the chromosomes with the highest fitness values to be the parents of the next generation is called selection. There are different ways to achieve this, all of which include giving more probability of selection to the individuals with the highest fitness and then using a random selection. In this paper, a roulette wheel method was used for selection. Next is crossover, which is the random pairing of chromosomes chosen in the selection stage to create children for the next generation. This is done by randomly exchanging some genomes (each gene represents a variable) of the chromosomes [86].

There is another mechanism called mutation, which helps diversify

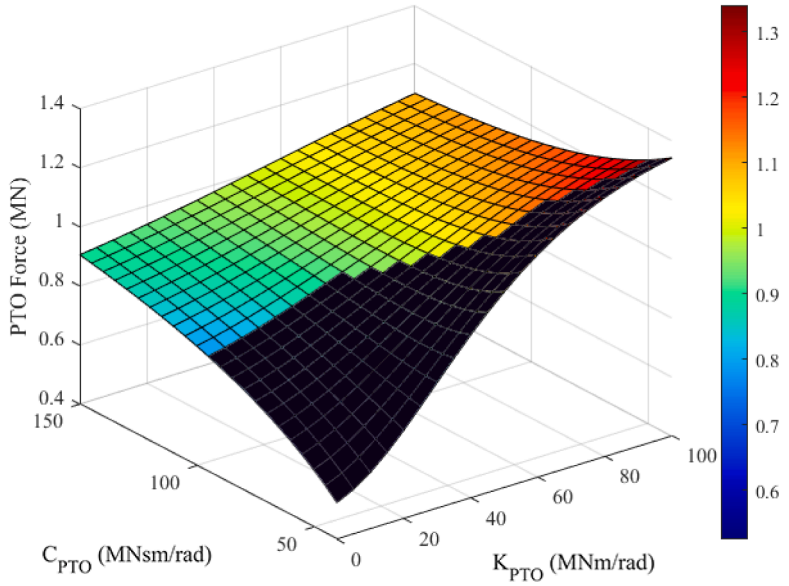

Fig. 9. Sensitivity analysis result of the effects of PTO parameters on the PTO force. Unfeasible values, shown in black, are excluded from the analysis.

the population. In it, some genes in chromosomes are changed randomly. Mutation ensures more exploration and prevents premature convergence. Finally, elitism preserves the best chromosomes from change and moves them to the next generation [86].

3.2. The particle swarm optimizer (PSO)

Particle swarm optimization (PSO) algorithm is a stochastic optimization technique that imitates the social behaviour of different animals, birds, and fishes. These animals cooperate in a social manner to find prey, and each member modifies its path based on its and the swarm's experiences. Each search agent tries to find the best solution based on 3 factors: its velocity, personal best solution, and the global best solution [87]. Here are the brief formulation of this algorithm:

$$v_{k+1_i} = \omega v_{k_i} + C_1 \cdot \text{rand} \cdot (g_k - x_{k_i}) + C_2 \cdot \text{rand} \cdot (p_k - x_{k_i}) \tag{1}$$

$$x_{k+1_i} = x_{k_i} + v_{k+1_i} \tag{2}$$

in which, v_{k_i} and x_{k_i} are the velocity and position of particle k, v_{k+1_i} and x_{k+1_i} are the velocity and position of particle k + 1, ω, C_1, and C_2 are the control parameters, the g_k and p_k are the global and personal best, and *rand* is a random number between 0 and 1. The GA [88] and the PSO [89] are of the most popular optimization algorithms that have been used in the field of renewable energy [90]

3.3. The artificial Gorilla Troops Optimizer (GTO)

The artificial Gorilla Troops Optimizer (GTO) is a new metaheuristic algorithm inspired by the social intelligence of gorilla troops in nature. In this algorithm, 5 different strategies are used to mathematically present the social behaviors of gorillas via optimization mechanisms, namely exploration and exploitation. Three of these tactics are for exploration: migration to unidentified places, moving to other gorillas, and migration to identified places. On the contrary, two strategies are used for exploitation, which are following the silverback and competition for adult females. The silverback gorillas act as the leaders of the group; they make decisions and guide the other gorillas, but as they age, they are replaced with younger gorillas. An extensive formulation and benchmarking of this algorithm is presented in [91].

3.4. The standard GWO

The Grey Wolf Optimizer (GWO) is a bio-inspired algorithm based on a grey wolf breed's leadership hierarchy and hunting behaviour. Mirjalili et al. [92] simplified their hunting mechanism and introduced four types of wolves, the alpha (α), the beta (β), the delta (δ), which are, respectively, the best solutions of the algorithms (have the best knowledge about the location of the optimum) and the omegas (ω) which comprise the rest of the pack and follow the three aforementioned wolves to get closer to the prey.

We can show the encircling of the prey process mathematically using the following equations:

$$\overrightarrow{D} = \left| \overrightarrow{C} . \overrightarrow{X_p}(t) - \overrightarrow{X}(t) \right| \tag{3}$$

$$\overrightarrow{X}(t+1) = \overrightarrow{X_p}(t) - \overrightarrow{A} . \overrightarrow{D} \tag{4}$$

in which t is the current iteration, $\overrightarrow{X}$ indicates the position of a grey wolf, $\overrightarrow{X_p}$ is the position of the prey, and $\overrightarrow{A}$ and $\overrightarrow{C}$ are coefficient vectors.

The $\overrightarrow{A}$ and $\overrightarrow{C}$ vectors are determined as follows:

$$\overrightarrow{A} = 2\overrightarrow{a} . \overrightarrow{r_1} - \overrightarrow{a} \tag{5}$$

$$\overrightarrow{C} = 2 . \overrightarrow{r_2} \tag{6}$$

in which $\overrightarrow{a}$ linearly decreases from 2 to 0, and $\overrightarrow{r_1}$ and $\overrightarrow{r_2}$ are random numbers between 0 and 1.

As stated, the ω wolves update their positions based on the three best search agents (α, β, and δ wolves). They follow these equations:

$$\overrightarrow{D_\alpha} = \left| \overrightarrow{C_1} . \overrightarrow{X_\alpha} - \overrightarrow{X} \right| \tag{7}$$

$$\overrightarrow{D_\beta} = \left| \overrightarrow{C_2} . \overrightarrow{X_\beta} - \overrightarrow{X} \right| \tag{8}$$

$$\overrightarrow{D_\delta} = \left| \overrightarrow{C_3} . \overrightarrow{X_\delta} - \overrightarrow{X} \right| \tag{9}$$

$$\overrightarrow{X_1} = \overrightarrow{X_\alpha} - \overrightarrow{A_1} . \left(\overrightarrow{D_\alpha} \right) \tag{10}$$

$$\overrightarrow{X_2} = \overrightarrow{X_\beta} - \overrightarrow{A_2}.\left(\overrightarrow{D_\beta}\right) \tag{11}$$

$$\overrightarrow{X_3} = \overrightarrow{X_\delta} - \overrightarrow{A_3}.\left(\overrightarrow{D_\delta}\right) \tag{12}$$

$$\overrightarrow{X}\left(t+1\right) = \frac{\overrightarrow{X_1}\left(t\right) + \overrightarrow{X_2}\left(t\right) + \overrightarrow{X_3}\left(t\right)}{3} \tag{13}$$

This was a simple overview of GWO's origin and mechanism.

3.5. Modified GWO (mGWO)

Mittal et al. [93] believed that the linear equation of the a does not provide a good balance between exploration and exploitation, so they tried this nonlinear equation:

$$\overrightarrow{a} = 2\left(1 - \frac{t^2}{T^2}\right) \tag{14}$$

in which t represents the current iteration, and T is the total number of iterations. This equation resulted in 70% exploration and 30% exploitation of the total iterations.

3.6. Exploration-enhanced GWO (EEGWO)

Since in GWO, all the search agents gravitate toward the three best solutions, this algorithm can be susceptible to premature convergence. Therefore, Long et al. [94] modified the position-updating equation inspired by the PSO algorithm to emphasize more on the exploration:

$$\overrightarrow{X}\left(t+1\right) = b_1.r_3.\frac{\overrightarrow{X_1}\left(t\right) + \overrightarrow{X_2}\left(t\right) + \overrightarrow{X_3}\left(t\right)}{3} + b_2.r_4.\left(\overrightarrow{X} - \overrightarrow{X}\right) \tag{15}$$

where $\overrightarrow{X}$ is another randomly selected search agent from the population, r_3 and r_4 are random numbers in [0,1], and $b_1, b_2 \in (0,1]$ indicate constant coefficients to balance the exploration/exploitation (in the mentioned study the selected values are $b_1 = 0.1$ and $b_2 = 0.9$).

They also proposed a new formula for the control parameter $\overrightarrow{a}$:

$$\overrightarrow{a} = a_{initial} - \left(a_{initial} - a_{final}\right).\left(\frac{T-t}{T}\right)^{\mu} \tag{16}$$

where μ is the nonlinear modulation index ($\mu = 1.5$ in the aforementioned study), and $a_{initial}$ and a_{final} are 2 and 0, respectively.

3.7. Improved GWO (IGWO)

In order to address the challenges associated with the conventional Maximum Power Point Tracking (MPPT) techniques, which is the power maximization of the PV system [95], and improving their efficiency in finding the global maximum power point, Ma et al. [96] utilized the fitness value of the search agents for their position-updating mechanism as follow:

$$\overrightarrow{X}\left(t+1\right) = \begin{cases} \frac{f_\alpha.\overrightarrow{X_1}}{f} + \frac{f_\beta.\overrightarrow{X_2}}{f} + \frac{f_\delta.\overrightarrow{X_3}}{f}, & f_i \leqslant f_{avg} \\ \frac{\overrightarrow{X_1} + \overrightarrow{X_2} + \overrightarrow{X_3}}{3}, & f_i > f_{avg} \end{cases} \tag{17}$$

$$f = f_\alpha + f_\beta + f_\delta \tag{18}$$

where f_α, f_β, and f_δ are fitness values of α, β, and δ, respectively. f_{avg} is the average of these 3 fitness values, and f_i is the fitness value of grey wolf individuals.

The authors modified the $\overrightarrow{a}$ formula as well:

$$\overrightarrow{a} = a_{min} + \left(a_{max} - a_{min}\right).\left(1 - \frac{t}{T}\right)^2 \tag{19}$$

where a_{min} and a_{max} are 0 and 2, respectively.

3.8. Efficient and robust GWO (ERGWO)

With the intention of tackling large-scale numerical optimization problems, Long et al. performed another study to enhance the performance of the GWO [97]. Following the footsteps of the previous studies, they changed both the position-updating equation and the $\overrightarrow{a}$ equation. The first change can be seen below, where they used a proportional weighting method similar to [96]:

$$w_1 = \frac{\left|\overrightarrow{X_1}\right|}{\left|\overrightarrow{X_1}\right| + \left|\overrightarrow{X_2}\right| + \left|\overrightarrow{X_3}\right|} \tag{20}$$

$$w_2 = \frac{\left|\overrightarrow{X_2}\right|}{\left|\overrightarrow{X_1}\right| + \left|\overrightarrow{X_2}\right| + \left|\overrightarrow{X_3}\right|} \tag{21}$$

$$w_3 = \frac{\left|\overrightarrow{X_3}\right|}{\left|\overrightarrow{X_1}\right| + \left|\overrightarrow{X_2}\right| + \left|\overrightarrow{X_3}\right|} \tag{22}$$

$$\overrightarrow{X}\left(t+1\right) = \frac{1}{w_1 + w_2 + w_3}.\frac{w_1.\overrightarrow{X_1} + w_2.\overrightarrow{X_2} + w_3.\overrightarrow{X_3}}{3} \tag{23}$$

where w_1, w_2, and w_3 are the learning rate of ω wolves from α, β, and δ wolves, respectively. The $\overrightarrow{a}$ changes following this formula:

$$\overrightarrow{a} = a_{initial} - \left(a_{initial} - a_{final}\right).\mu^{-t} \tag{24}$$

where $a_{initial}$ and a_{final} are 2 and 0, respectively. $\mu \in [1.0001, 1.005]$ is the nonlinear modulation index (in the mentioned study $\mu = 1.001$).

3.9. Hill-climbing exploraitive GWO (HC-EGWO)

The Gray Wolf Optimizer (GWO), although remarkable in its performance for solving diverse optimization problems [92], is not without its shortcomings. Primarily, it is prone to premature convergence towards local optima in the search space, specifically during complex, high-dimensional problems [98]. This challenge arises due to the declining exploration rate (parameter $\overrightarrow{a}$) in the original GWO algorithm, which transitions from 2 to 0 linearly. While this allows the algorithm to either explore or exploit optimal solutions when $\overrightarrow{a}$ is above 1, it leads to exploitation when $\overrightarrow{a}$ is below 1, thereby accelerating convergence towards local optima.

In addressing this limitation, we propose the Explorative Gray Wolf Optimizer (EGWO), a novel enhancement to the original GWO that amplifies the exploration rate by modifying the parameter $\overrightarrow{a}$. In EGWO, $\overrightarrow{a}$ is altered as per the equations:

$$R = \left(\frac{T-t}{T-1}\right), \tag{25}$$

$$\overrightarrow{a} = 2.\left(1 - \left(e^{\left(t^R - T^R\right)}\right)\right) \tag{26}$$

where t is the current iteration, and T is the maximum number of iterations. This modification empowers the algorithm to delay the convergence process and explore the search space more thoroughly, reducing the chance of being trapped in local optima. Furthermore, to fortify the global search capabilities of EGWO, we propose a robust hybrid algorithm that incorporates a Random-restart hill-climbing local search,

dubbed HC-EGWO. Fig. 10 shows the evolution of $\vec{a}$ throughout the iterations for each of the six optimization approaches. Also, the Exploration Ratio (ER) is presented for each method; this value shows how much of the search process is allocated to potential exploration in GWO. By comparing the values, it is clear that HC-EGWO has the best ER value and the most potential to search the unexplored areas of the search space thoroughly.

In this hybrid scheme, EGWO operates on a superior level to create a global track and procure an array of suitable solutions. When the EGWO encounters stagnation or converges prematurely towards a local optimum, the hill-climbing algorithm initiates a local search around the best solution found by the upper level (EGWO). It does so by creating a comprehensive neighbourhood search, thereby preparing to escape such unfavourable scenarios.

The performance threshold is computed as follows:

$$\Delta Best_{THD} = \frac{\sum_{k=1}^{M}\left(Best_{THD_k} - Best_{THD_{k-1}}\right)}{M} \tag{27}$$

where $Best_{THD}$ is the optimal solution found per generation, and M is tied to the range of iterations to determine the average EGWO performance. When the solution offered by the local search outperforms the initial one, EGWO's global best is updated.

The HC-EGWO algorithm iteratively executes the hill-climbing process whenever the EGWO performance dips, each time establishing an initial condition to facilitate escape from undesirable circumstances. The search step size is decremented linearly as follows to achieve a fine balance between exploration and exploitation:

$$S_t = S_t - \left(\frac{t}{T}S_t\right) + 1 \tag{28}$$

Here, t and T denote the current and maximum iteration numbers, respectively, while S_t represents the neighborhood search's step size.

Algorithm 1 illustrates the detailed steps of the proposed optimization method (HC-EGWO). The initial solution encompasses wave height (H), wave period (T), PTO stiffness coefficient (K), and PTO damping coefficient (C).

One of the crucial parameters in the local search algorithm is g, which signifies the precision of the neighborhood search surrounding the globally optimal solution proposed by EGWO. A smaller step size for HC slows down the convergence speed. However, a larger step size bolsters the exploration capability, possibly at the expense of the exploitation capability, leading to the possibility of skipping over globally optimal or high-potential solution surfaces. For each decision variable, the neighborhood search evaluates two distinct direct searches, either incremental or decremental. After evaluating the generated solutions, the optimal candidate is chosen to iterate the search algorithm. It should be noted that the HC algorithm should not be employed during the initial iteration of the optimization process due to the pronounced tendency for converging to local optima. Moreover, for optimizing large-scale problems, HC may not be a suitable choice.

Algorithm 1. *Hill Climbing Explorative Gray Wolf Optimizer*

procedure HC-EGWO
$N = 30, D = 4$ ▷Population size and dimension size
$\mathbb{S} = \{\langle H_1, T_1, K_1, D_1\rangle, \ldots, \langle H_N, T_N, K_N, D_N\rangle\}$ ▷Initialize the population of wolves
$Checkiflb_1^N \leqslant \mathbb{S} \leqslant ub_1^N$
$Max_{iter} = 100$ ▷Maximum number of iterations
for $iter = 1, .., Max_{iter}$ **do**
$R = (Max_{iter} - iter)/(Max_{iter} - 1)$
$\vec{a} = 2 \cdot (1 - e^{(iter^R - Max_{iter}^R)})$ ▷Calculate exploration rate $\vec{a}$ with the new formulation
Sort the population $\mathbb{S}$ based on fitness and get the leading wolves α, β, and δ
for $i = 1, .., N$ **do**
for $j = 1, .., D$ **do**

(*continued on next column*)

(*continued*)

Calculate A_{ij} and C_{ij} for each of the leading wolves
Update the position of the ith wolf in dimension j using the positions of α, β, and δ
end for
end for
Update the positions of α, β, and δ based on the updated population
$Best_{iter} = Max(\mathbb{S})$ ▷Get the best solution in this iteration
$\Delta Best = Best_{iter} - Best_{iter-1}$ ▷Calculate the difference between the best solutions in the current and previous iterations
if $\Delta Best < Th$ **then** ▷If the difference is less than a threshold Th, perform Hill Climbing
Initialize the constraints lb_1^d, ub_1^d
$S_1^d = (Min_1^d + Max_1^d)/g$ ▷Compute the step size, g is search resolution
$Sol_1 = \{\langle H, T, K, D\rangle\}$ ▷Initial solution
$(fitness_1) = Eval(Sol_1)$ ▷Evaluate the solution 24: **for** $iter \leqslant Max_{iter}$ **do**
$Te = Sol_{iter}$
while $t \leqslant len(Sol_1)$ **do**
$Te_t = Te_t \pm S_t$ ▷Neighborhood search
$(fitness_t^{iter}) = Eval(Te_t)$
$t = t + 1$
end while
$\langle Max_{fit}, Index_{max}\rangle = Max(fitness)$
$Sol_{iter} = Te_t(Index_{max})$ ▷Select the best feasible solution and update the design
$S_t = S_t - \left(\frac{iter}{Max_{iter}}S_t\right) + 1$ ▷S_t linearly reduced
end for
$Best_{iter} = Sol_{iter}$ 36: **end if**
end for
return $Best_{iter}$ ▷Return the best solution
end procedure

4. Problem formulation

4.1. Optimization problem

This study aims to maximize the power output of the OSWEC in the Caspian Sea climate by optimizing four decision variables: wave height, wave period, Power Take-Off damping (C), and Power Take-Off stiffness (K). The feasible ranges for C and K were determined through a comprehensive literature review and an initial sensitivity analysis. Additionally, wave data were gathered from the INIO.

4.2. Algorithms initial parameters

In this section, the initial parameters of the genetic algorithm and the grey wolf optimizer. In the case of the GA, due to the computationally expensive nature of our problem, only two parameters, the population size and the probability of crossover have been investigated, and other parameters have been chosen based on similar studies conducted in this field. The probability of mutation is set to 20% [99–101] and the elitism rate to 10% [99,102]. The crossover rate tested values were chosen from studies from Sharp et al. [99,103]. Finally the population sizes of 10 and 20 were selected to evaluate the impact of this parameter.

As for the GWO, the 3 population sizes (10, 20, and 30) were tested. In this study, six variants of the GWO have been studied, each one having a different mechanism for the control parameter a, taking different forms from linear to exponential. The effect of this parameter is visible in the performance of each one of these modifications. The tested initial parameters and their performance are given in Table 1. Based on the results, the initial values for starting these methods have been chosen, which are presented in Table 2.

4.3. The wave energy converter

As stated before, the Oscillating Surge WEC was chosen for this study due to multiple reasons. The OSWEC is fixed to the ground, and it

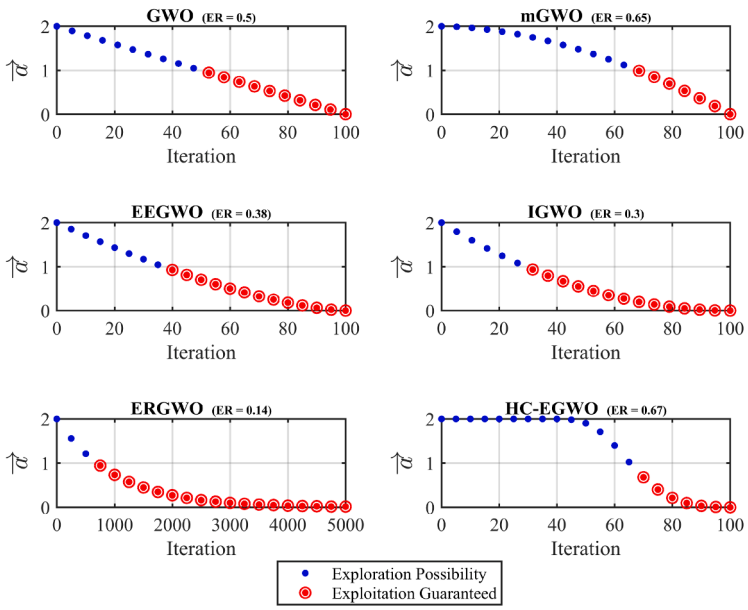

Fig. 10. The evolution of $\vec{a}$ value during the optimization process for the six evaluated GWO methods in this study, and their Exploration Ratio (ER).

Table 1
Effects of Initial Parameters of the GA and GWO algorithms on their performance.

Method			Population Size		
			10	20	30
GA	P_{cr}	80	902.04	885.20	870.3
		95	917.00	868.40	861.2
	GWO		1311.95	1329.12	1326.61

Table 2
Initial Parameters chosen for all the algorithms used in this study.

Method	Settings
GA	Npop = 10, $P_m = 0.2$, $P_{cr} = 0.95$, $E_r = 0.1$
PSO	Npop = 20, $C_1 = 2$, $C_2 = 1.5$, w = [0.2, 0.9]
GTO	Npop = 20, p = 0.03, $\beta = 3$, w = 0.8
GWO	Npop = 20

features a hinged connection between its base and flap. This hinge constrains the flap's movement, allowing it to pitch around the hinge point. The converter's physical dimensions at scale are shown in Fig. 11. Moreover, the OSWEC's flap has a mass of 127 tonnes, and its other properties are listed in Table 3.

Table 3
OSWEC's Flap Mass Properties [33]

Body	Direction	Center of Gravity (m)	I_{xx} (kg. m^2)	I_{yy} (kg.m^2)	I_{zz} (kg. m^2)
Flap	x	0	0	0	0
	y	0	0	1,850,000	0
	z	−3.9	0	0	0

4.4. WEC-Sim

WEC-Sim provides an open-source simulation tool for the community. In order to determine the dynamic response of the WEC system, the equation of motion for the device about its center of gravity in the time domain has to be solved [33]:

$$m\ddot{X} = F_{exc}(t) + F_{rad}(t) + F_{PTO}(t) + F_B(t) \quad (29)$$

where m is the mass matrix of the WEC, $\ddot{X}$ is the acceleration vector, $F_{exc}(t)$ is the wave excitation vector, $F_{rad}(t)$ is the force and torque vector caused by wave radiation, $F_{PTO}(t)$ is the PTO force and torque vector, and $F_B(t)$ is the net buoyancy restoring force and torque vector. The $F_{exc}(t)$ and $F_{rad}(t)$ are calculated using Boundary Element Method (BEM) solvers [104]. This module is developed on MATLAB/Simulink/Simscape. Fig. 12 shows the Simulink models of the proposed OSWEC

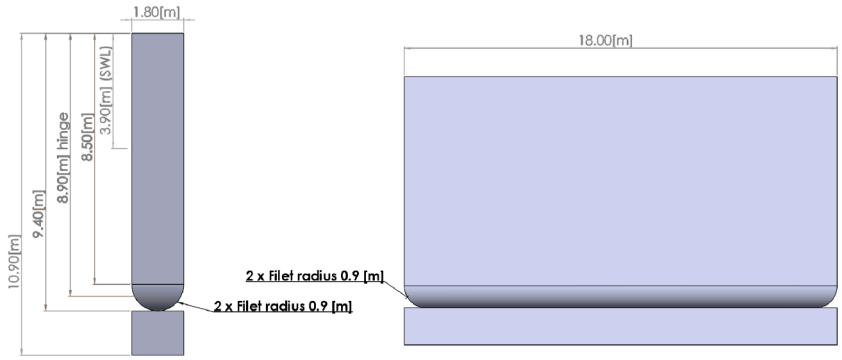

Fig. 11. OSWEC's full-scale detailed dimensions [.33].

Table 4
The details of optimization parameters and other variables related to the wave power simulation applied.

Abbreviation	Full name	Description
H	Height (m)	Measure of the amplitude or intensity of a wave
T	Period (s)	Time for completing one full cycle of wave
K	PTO Stiffness Coefficient (MNm/rad)	Relationship between the deformation of a PTO system and the force it generates
C	PTO Damping Coefficient (MNsm/rad)	Relationship between the PTO system's velocity and the force it generates
FlapEP	maxFlapExcitationPitch	Maximum Flap's Excitation Force (kN)
FlapRDP	maxFlapRDPitch	Maximum Flap's Radiation Damping Force (kN)
FlapAMP	maxFlapAMPitch	Maximum Flap's Added Math Force (kN)
FlapRP	maxFlapRestoringPitch	Maximum Flap's Restoring Force (kN)
ForceTPTOP	maxForceTotalPTOPitch	Maximum PTO's Force (kN)
meanFlapAVD	meanFlapAngularVelocityD	Average Flap's Velocity (degree/s)
maxFlapAVD	maxFlapAngularVelocityD	Maximum Flap's Velocity (degree/s)
FlapARD	maxFlapAngularRotationD	Maximum Flap's Rotation (degree)
Flapa	flap's acceleration (degree/s^2)	Affects the PTO system's structural integrity & overall performance.
Flapfam	flap's force added math (N)	
Flapfe	flap's excitation force (N)	A function of the displacement, velocity and acceleration of PTO system
Flapfr	flap's restoring force (N)	Result of the buoyancy and gravity forces acting on the WEC
Flapfrd	flap's radiation damping force (N)	Due to the interaction between a WEC and the surrounding water waves
Flapft	flap's total force (N)	Sum of hydrodynamic forces, gravity forces, buoyancy forces, and other forces generated by the PTO system.
Flapv	flap's velocity (degree/s)	Rate of change of the flap angle,
Flapx	flap's position (degree)	
PTOa	PTO's acceleration (degree/s^2)	Alteration rate of its velocity over time
PTOv	PTO's velocity (degree/s)	Alteration rate of its position over time
PTOf	PTO's force (N)	Is transmitted from the WEC to the PTO system due to the motion of the waves
PTOx	PTO's position (degree)	

investigated in this paper [33]. Moreover, irregular waves are simulated as a superposition of regular waves [105].

In WEC-Sim, the PTO unit can be characterized by a linear spring-damper system, in which the PTO force is calculated by:

$$F_{PTO} = K \cdot X + C \cdot \dot{X} \tag{30}$$

where K is the PTO stiffness coefficient, C is the PTO damping coefficient, and X and $\dot{X}$ are the relative motion and velocity between the flap and the base of the OSWEC. Since the studied device is fixed to the bed, X and $\dot{X}$ can be considered the flap's motion and velocity. Next, the power output of the PTO can be obtained by the following [33]:

$$P_{PTO} = F_{PTO} \cdot \dot{X} = K \cdot X \cdot \dot{X} + C \cdot \dot{X}^2 \tag{31}$$

In WEC-Sim, the regular wave excitation force after the ramp time (the necessary time for the system to stabilize from the starting stage of the simulation) is obtained from the:

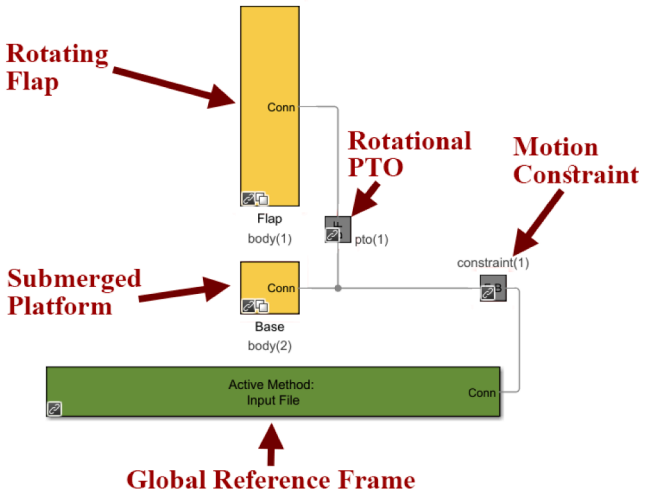

Fig. 12. OSWEC's Simulink model in WEC-Sim [.33].

$$F_{exc}\left(t\right) = \Re\left[\frac{H}{2} F_{exc}\left(\omega, \theta\right) e^{i\omega t}\right] \tag{32}$$

where $\Re$ denotes the real part of the term in bracket, H is the wave height, F_{exc} is the frequency dependent complex wave-excitation amplitude vector, and θ is the wave direction. The excitation force in irregular sea states can be calculated as follows:

$$F_{exc}\left(t\right) = \Re\left[\sum_{j=1}^{N} F_{exc}\left(\omega_j, \theta\right) e^{i(\omega t + \phi)} \sqrt{2S(\omega_j) d\omega_j}\right] \tag{33}$$

where N is the number of frequency bands that discretizes the wave spectrum, ϕ is the randomized phase angle, and $S(\omega)$ is the distribution of wave energy over a range of wave frequencies that are characterized by a H_s and T_p.

The software uses the following equation to calculate the radiation terms, namely the added mass and the radiation-damping torques. This equation utilizes the convolution integral formulation based on the Cummins equation to take the fluid memory effect into consideration. In this equation, the first term is the added mass torque, and the second term is the radiation-damping torque:

$$F_{rad}\left(t\right) = -A_{\infty}\ddot{X} - \int_0^t K_r\left(t-\tau\right)\dot{X}\left(\tau\right) d\tau \tag{34}$$

where A_∞ is the added mass matrix at an infinite frequency, and K_r is the radiation impulse response function, which is calculated by this equation:

$$K_r t = \frac{2}{\pi}\int_0^{\infty} B\left(\omega\right)\cos\left(\omega t\right) d\omega \tag{35}$$

Notably, the assumption is that there is no motion before t $= 0$. The A_∞ and $B(\omega)$ coefficients are calculated by the NEMOH, the BEM solver WEC-Sim uses. Finally, The buoyancy term F_B depends on three factors: the hydrostatic stiffness coefficient and displacement and mass of the body.

4.5. Optimization run details

In order to optimize the performance of an OSWEC in the southern Caspian Sea, WEC-Sim was used to simulate the converter and HC-EGWO to optimize its power output. A simulation time of 400 s and a ramp time of 100 s were chosen, with time steps of 0.1 s. Furthermore, ten optimization runs using HC-EGWO were performed, each with 1000 iterations and 20 search agents. Moreover, the Joint North Sea Wave

Table 5
The best solution of GA, PSO, GTO, original GWO, our proposed hybrid solution (last row), and other modifications in optimizing PTO coefficients and wave conditions. Forces exerted on the flap and the averaged power output are also reported per case.

	H	T	K	C	FlapEP	FlapRDP	FlapAMP	FlapRP	ForceTPTOP	FlapARD	AvgPower
GA	3.87	7.31	25.58	113.40	3487.3	1273.5	551.79	670.78	34960	19.88	917.006
PSO	4.22	7.83	33.04	90.03	3451.8	1479.9	617.14	773.99	35028	22.94	1283.598
GTO	4.22	7.82	47.92	82.08	3427.6	1562.7	678.92	836.87	37931	24.80	1319.498
GWO	4.22	7.40	54.53	76.96	3688.8	1497.4	709.40	834.93	38289	24.74	1325.008
mGWO	4.22	7.40	56.19	74.78	3712.6	1513.9	730.57	848.27	38942	25.14	1326.068
EEGWO	4.22	7.69	51.62	80.92	4192.1	1640.3	753.18	908.92	41462	26.93	1290.216
IGWO	4.22	7.43	54.41	75.77	3771.9	1550.6	742.19	855.93	39114	25.36	1329.108
ERGWO	4.22	7.40	55.34	75.62	3684.2	1513.4	721.58	846.14	38352	25.07	1331.921
HC-EGWO	4.22	7.39	54.46	75.58	3686.9	1512.5	722.27	842.49	38306	24.97	1332.955

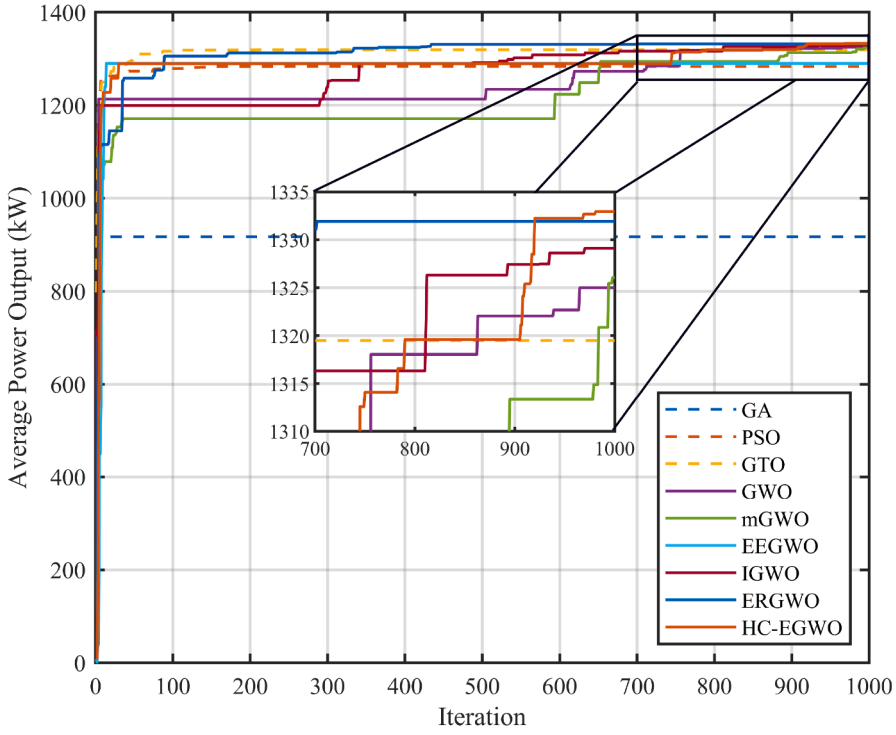

Fig. 13. The convergence curves for the average performance of GA, the conventional GWO, its four modifications, and the proposed algorithm in this study.

Project (JONSWAP) was chosen as the wave spectrum representing the Caspian Sea's wave states [106,107].

5. Results

5.1. Algorithms performance in the defined problem

Here, the proposed algorithm was compared to Genetic Algorithm, the PSO, the GTO, the conventional GWO, and its four variants that were introduced earlier. Each algorithm was run ten times with a population size of 20 and 1000 iterations to achieve maximum power output except the GA, which had the same number of evaluations but only a population size of 10. The GA result is scaled to be parallel to other methods in terms of the number of evaluations done at each point of the convergence curve. Table 5 shows the critical parameters of the OSWEC in the performance of each algorithm.

As can be seen in Table 5, all the algorithms, except the GA, have competitive performances; however, the proposed algorithm (HC-EGWO) yields better results than all of them. HC-EGWO can improve the power output by 0.08% up to 3.31% compared to the other GWO variants and 45% increase over the GA. Moreover, the EEGWO has the worst performance among the GWO modifications. The PSO and GTO methods both showed great performance but not enough to surpass the GWO. Next, the convergence curves for the nine inspected algorithms are presented in Fig. 13.

Fig. 13 shows how competitive all methods were in this problem and how only the GA was unable to find high-performing solutions. In addition, all these algorithms were able to reach high amounts of average power output in under 50 iterations.

5.2. Wave and PTO parameters optimization

In this section, the results of the wave and PTO parameters optimization of the oscillating wave surge converter are presented. In order to get a better understanding of the effects of optimization on performance, the converter's functioning and outputs in 3 scenarios are analyzed and compared. One of the cases is the scenario with the best-found solution by the HC-EGWO (Case C). Next, the case with the default WEC-Sim parameters was chosen to see how much improvement the input fine-tuning has achieved (Case A). However, since the default WEC-Sim case parameters were in the unfeasible area following the literature review this study performed at the research's beginning, another scenario was added for evaluation. It was observed that the PTO damping with a value of 0.012 MNsm/rad was in the unfeasible area, so based on the literature review and the initial sensitivity analysis, the minimum feasible value, which was 90 MNsm/rad, was chosen for the following

Table 6
The details of the 3 analyzed cases in this study

Case A	H	T	K	C	FlapEP	FlapRDP	FlapAMP
	2.5	8	0	0.012	1624	1778	691.7
	FlapRP	ForceTPTOP	meanFlapAVD	maxFlapAVD	FlapARD	MaxPower	AvgPower
	887.4	4.158	7.049	19.85	26.29	1.440	0.228
Case B	H	T	K	C	FlapEP	FlapRDP	FlapAMP
	2.5	8	0	90	1624	780.3	297.6
	FlapRP	ForceTPTOP	meanFlapAVD	maxFlapAVD	FlapARD	MaxPower	AvgPower
	360.6	13395	2.733	8.527	10.686	1993	287.7
Case C	H	T	K	C	FlapEP	FlapRDP	FlapAMP
	4.223	7.39	54.46	75.58	3687	1512	722
	FlapRP	ForceTPTOP	meanFlapAVD	maxFlapAVD	FlapARD	MaxPower	AvgPower
	842	38306	3.82	21.92	24.97	13393.98	1332.95

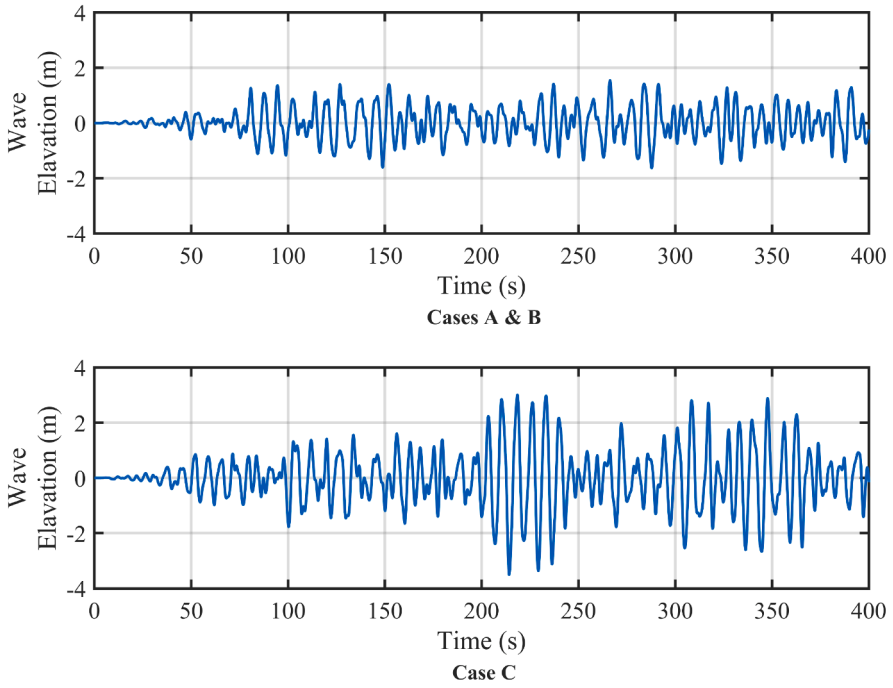

Fig. 14. Wave elevation profile during the performance of the WEC for the 3 cases.

case, and the three other parameters stayed the same (Case B).

Table 6 presents the inputs, forces, oscillation, and power of the system in the three analyzed cases in detail. First, the wave elevation during the simulation for the 3 cases is presented in Fig. 14 in order to analyze the other parameters more effectively.

Next, the resulting oscillation details, PTO force, and power output will be inspected. As stated before, cases A and B have the same wave conditions. Hence, one wave elevation graph is plotted to represent the sea state in both cases in Fig. 14. According to this figure, in cases A and B, wave elevation relatively stays in the same range, and the amplitude does not change drastically at any point during the simulation. On the other hand, in case C, especially after the halfway mark, wave heights are greater and reach their maximum absolute value at around the 215-s mark. As previously mentioned, when using linear PTO for the OSWEC, WEC-Sim calculates the power output by multiplying the PTO force by the flap's angular velocity. Both the flap's motion and its angular velocity positively dictate the device's power output, which is this study's main objective.

First, we compare the flap's oscillation in cases A and B in Fig. 15. Since these two have the same wave characteristics but different PTO configurations, one can assign almost all the difference in oscillation to the PTO stiffness and damping. Both parameters are virtually trivial in case A and come into effect in case B. It can be seen that the PTO C and K in isolation dampen the flap's oscillations, both the motion and the velocity. For case C, the flap's fluctuation during the simulation almost mimics the shape of the wave elevation, which is predictable. But the maximum flap motion roughly occurs in $t = 125$ s of case A.

Next, in Fig. 16 the PTO force and power output for the 3 cases are presented. Note that for this purpose, the y-axis for the 3 cases is modified for more clear visualization. According to the y-axis, it can be said that roughly case B produces ten times more power the case A produces. And that case C generates 50 times more the case A.

Since case C is the best-found solution and has more prominent and more significant values, it is inspected first. For case C, the PTO force is peaking during the 200 s and 250 s marks due to the substantial wave magnitude (see Fig. 14). This happens multiple times to a lesser extent at different times during the simulation (100–140 s, 155–165 s, 175–180 s, 270–375 s). Similarly, it can be seen for case B that the highest power outputs occur when the PTO force is at max. But overall, the extent of the produced power is about five times smaller, which can be attributed to the PTO mechanical parameters. Finally, for case A, the default WEC-Sim case, considering the PTO stiffness coefficient is zero, and the

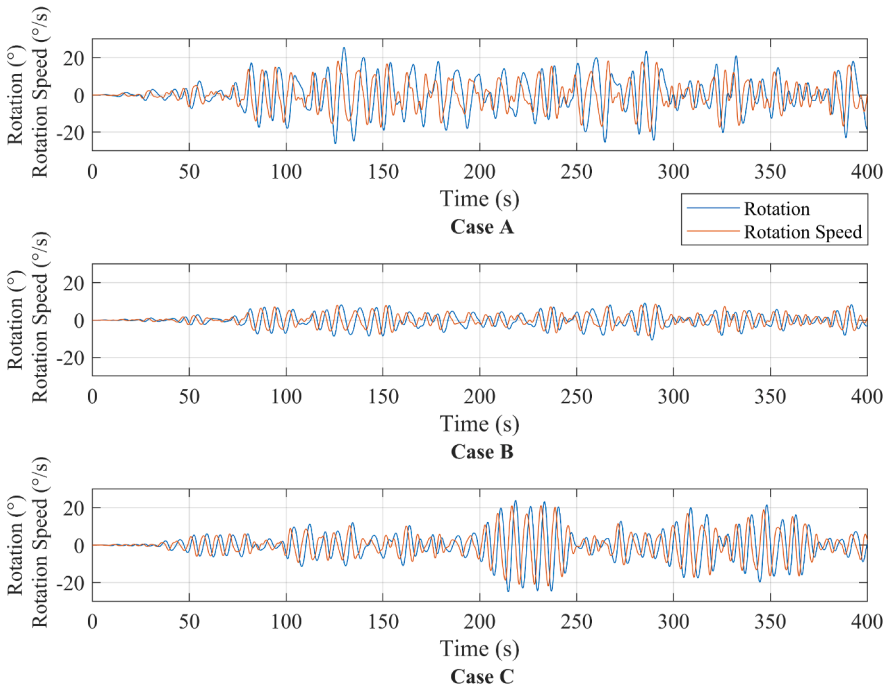

Fig. 15. Flap's oscillations motion and velocity the 3 cases.

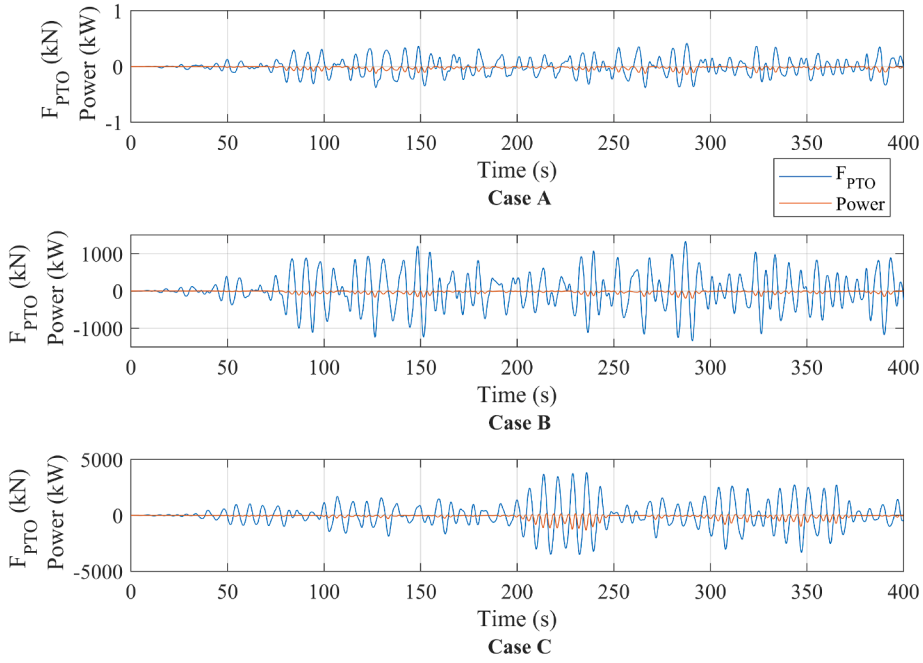

Fig. 16. PTO force and power output for the 3 cases.

damping coefficient is very low, the generated power is almost between 500 and 1000 times smaller than the best-found sample in case C. In the context of optimizing the power output of a WEC, parallel coordinate plots can be helpful in understanding the relationships between the optimization parameters (such as damping, stiffness, wave height, and period) and the resulting power output. For example, in Fig. 17, we can observe that increasing the damping and stiffness of the WEC leads to a decline in power output, while increasing the wave height leads to an upsurge in power output.

Fig. 17 showcases the parallel plots for the two selected runs of the HC-EGWO in order to achieve the highest power output; this includes the best-found solution by all the ten optimization runs. Furthermore, by analyzing the lines corresponding to each parameter in this Figure, it can be achievable to identify the range of parameter values that lead to optimal power output; for instance, the optimal ranges of K and C are [50–65,70–80], respectively. Another significant observation from the parallel plots is that there are sharp, non-linear relationships between the optimization parameters and the power output of the WEC.

Fig. 18 shows the parallel plots for the three scenarios studied in the result (See Section 5.2). These data are in real-time during the simulation time. Next, all the y-axis, except for the power output, are symmetrical, showcasing the device's oscillating nature and, therefore, its

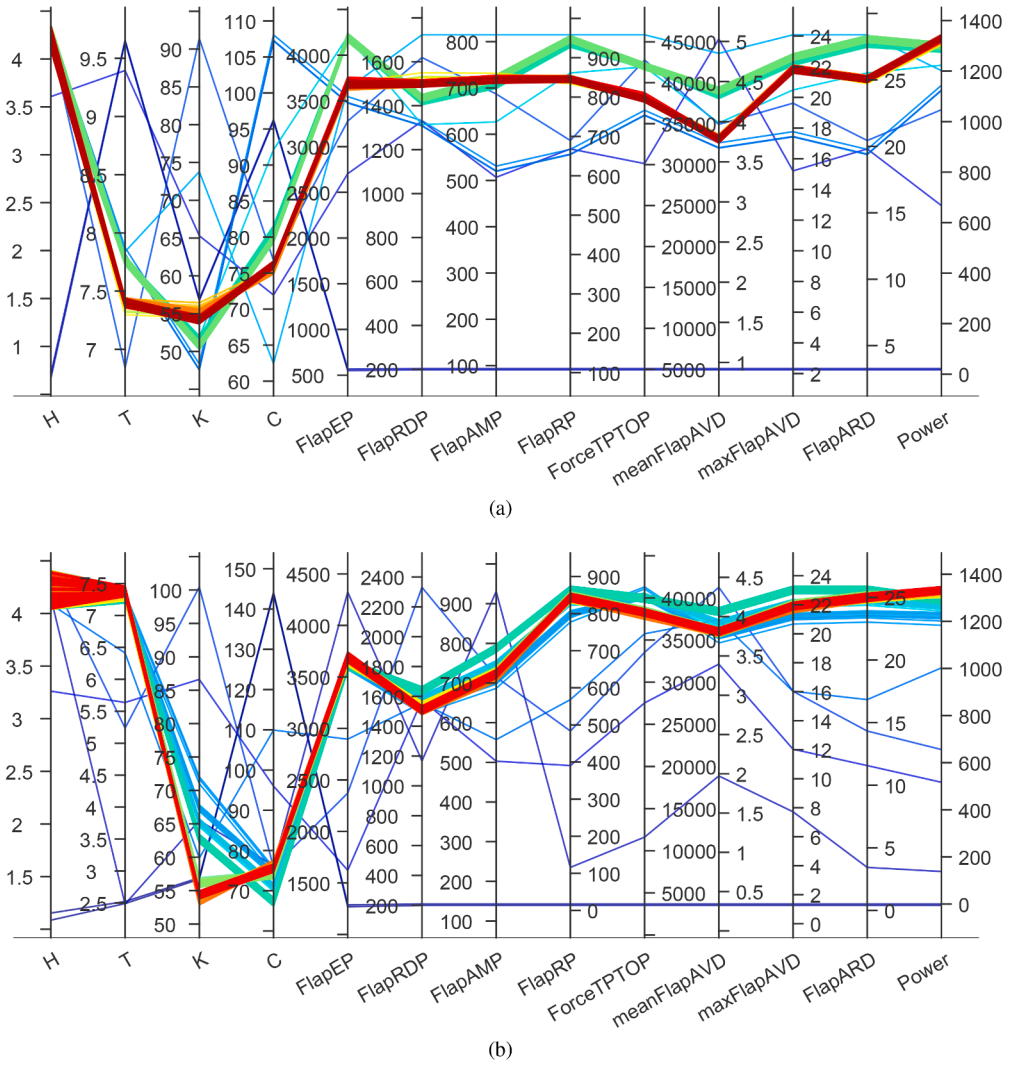

Fig. 17. Two examples of the best-performed optimization method's exploration through the decision variables (H, T, K, and C) with internal parameters of the simulator listed in Table 4, plus the average of total power output distribution visualized by a parallel coordinates plot. The dark red lines indicate the highest absorbed power output based on the configurations. (in the figures, the H, T, K, and C are the input parameters. FlapEP, FlapRD, and FlapAMP are, respectively, the excitation, radiation damping, and added mass torques, and the ForceTPTOP is the PTO force. The meanFlapAVD and maxFlapAVD are the average and maximum angular velocity of the flap, the FlapARD is the flap's angular rotation of the flap, respectively, and the Power is the average power output .of the system.).

parameters. But when taking a closer look at case A (Fig. 18(a)), it is visible that the only parameters that have the simultaneous maximum as the power output (red lines) are the flap's angular velocity and PTO force, this is consistent with equations for calculating the power output in WEC-Sim in earlier sections of the study. And also corresponds to the moderate values of the flap's acceleration, restoring torque, excitation torque, and other hydrodynamic forces. Based on case C (Fig. 18(c)), it can be seen that low absolute values of excitation force correspond to low power. Since both these parameters positively correlate with wave height, that is consistent with the theory. Notably, not every hydrodynamic force has the same trajectory as the power; for instance, the restoring force's maximum absolute values coincide with the lowest power outputs. Since the flap's restoring torque is dependent on the flap's displacement only, we can see that the displacement alone can not lead to the best performance. The flap's velocity can be considered a more critical and deciding factor.

5.3. Sensitivity analysis

Sensitivity analysis is a crucial mechanism in post-processing optimization methods due to identifying the most significant factors affecting the efficiency of the optimized models [108]. Table 6-Case C reports the best configuration of decision variables (H, T, K, and C) and internal hydrodynamic parameters of the simulator proposed by the HC-EGWO. Meanwhile, the sensitivity analysis results can be seen in Fig. 19. The black lines show the unfeasible areas of the search space for K (Fig. 19C (Fig. 19 power output of the best-found solution discovered by sensitivity analysis was 1333.1 (kW). This negligible improvement can confirm that the proposed optimization method (HC-EGWO) is able to explore comprehensively the search space and converge to an appropriate solution.

5.4. Regional site selection

In the last segment, an operational site will be selected as the best location for the installation of the device. This is obtained by analyzing the best-found solution and finding the location from the 105 initial data points in the Caspian Sea that has the closest wave characteristic values, namely wave height and wave period, to the theoretic best location. The optimum values are H = 4.223 m and T = 7.39 s. Then, the best location was found using a Root Mean Square Error method (Fig. 20), and the RMSE values for all the data points were evaluated. In the end, a data

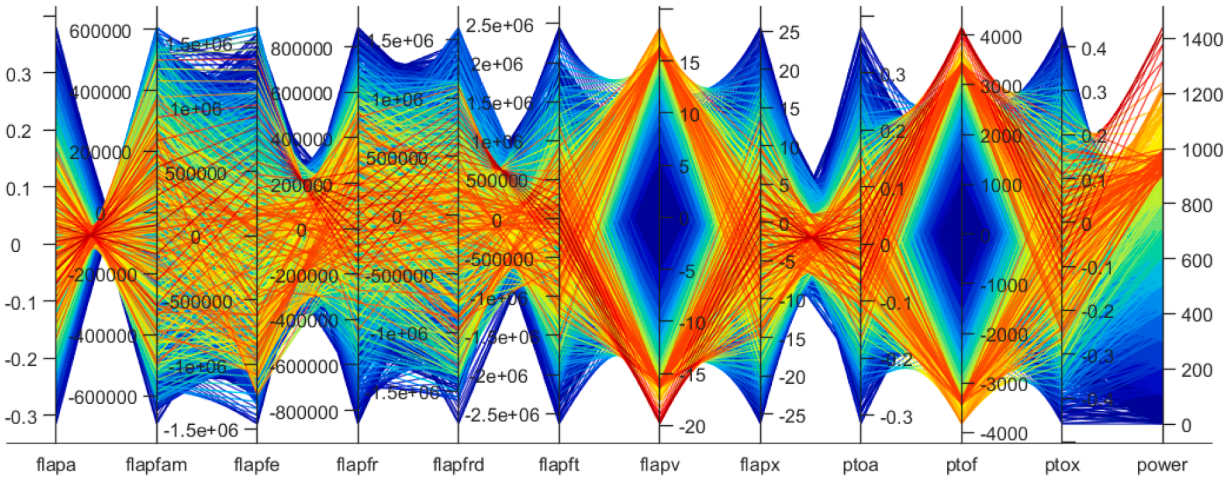

(a)

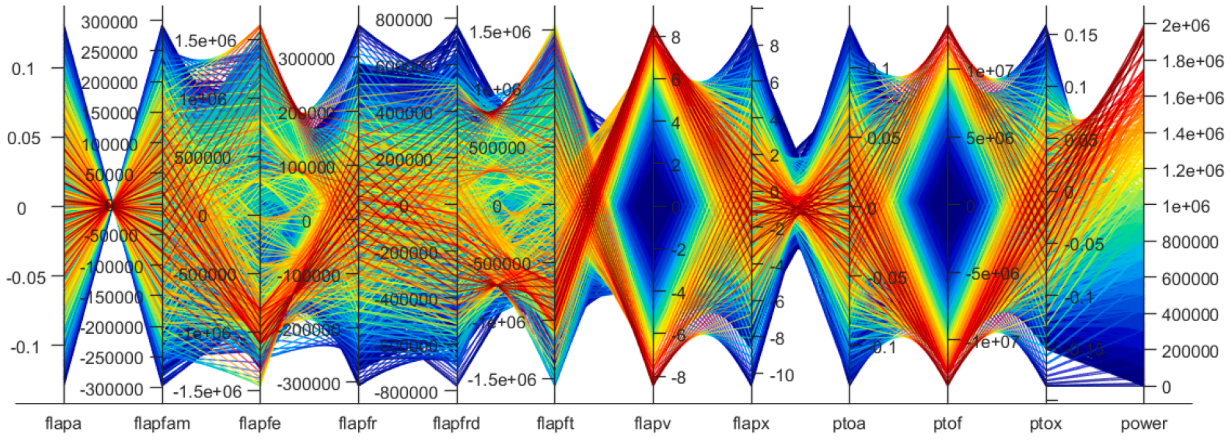

(b)

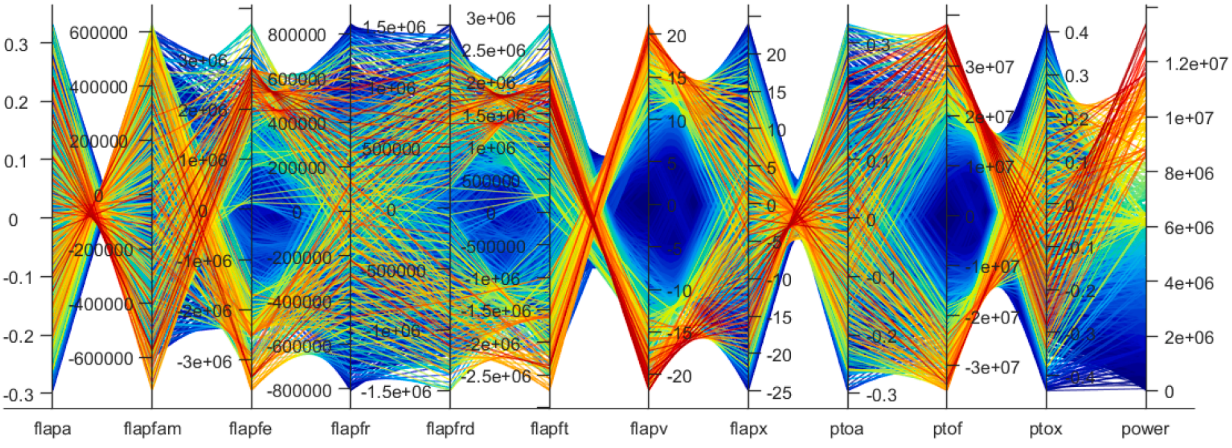

(c)

Fig. 18. Parallel interactions plot for the average of total power output distribution based on three scenarios described in the Result section. The technical details of the variables are listed in Table 4.

point belonging to the Kiashahr Port resulted in RMSE = 2.78, which was the minimum among the analyzed spots. The longitude and latitude of the best-found location are 37.6° N 50.1° E; this spot belongs to the Kiashahr Port.

6. Conclusion

This study focused on optimizing the Power Take-Off (PTO) parameters and site selection for an offshore Oscillating Surge Wave Energy Converter (OSWEC) in the Caspian Sea. The optimization was performed using the novel Hill Climbing Explorative Grey Wolf Opti-

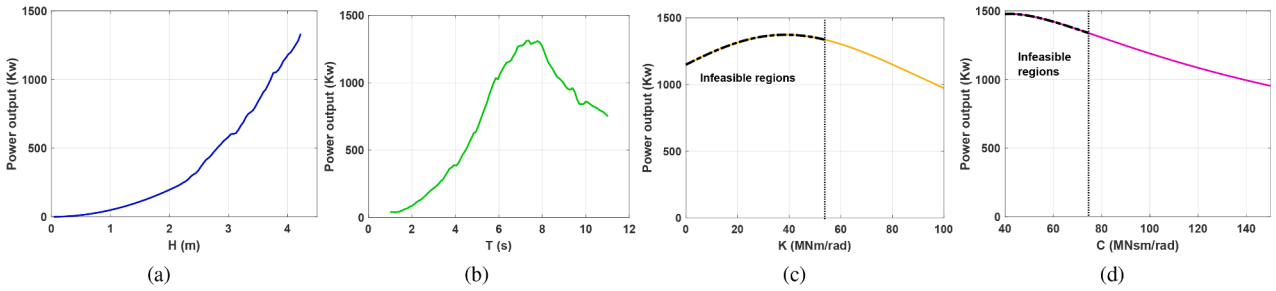

Fig. 19. Sensitivity analysis of the best-found configuration using the proposed hybrid optimization method.

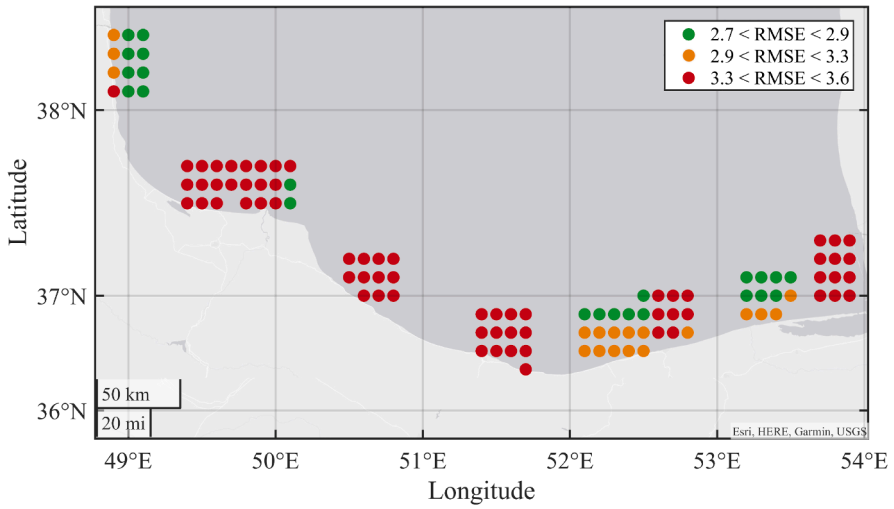

Fig. 20. Categorization of the 105 data points based on the fitness of their wave significant height and peak period (using the RMSE method).

mizer (HC-EGWO), which showed strong performance across 16 benchmark multimodal functions. When applied to the OSWEC case study, the HC-EGWO discovered a high-quality solution that increased the power output by approximately 3% compared to other GWO modifications and a substantial 45% increase over the genetic algorithm.

The results provide valuable insights into the complex interplay between the converter's mechanical design and the surrounding wave climate. Specifically, the initial sensitivity analysis revealed that wave height and PTO damping have the most substantial impact on the power output. Increasing the wave height boosts the absorbed power, while lower PTO damping is preferable. Meanwhile, moderate values of wave period and PTO stiffness lead to the highest outputs. There are also nonlinear relationships and trade-offs between the parameters influencing the hydrodynamic forces acting on the device. Overall, the proposed HC-EGWO algorithm proved effective in handling this challenging multimodal optimization problem. The hybridization with local search prevented premature convergence and bolstered the exploration of the solution space. The outcomes showcase the method's capabilities for optimizing offshore renewable energy systems where complex hydrodynamic interactions are involved. They provide a valuable starting point for devising control strategies that ensure OSWECs operate safely within extreme seas while maximizing power generation. Moreover, the results offer insights into deploying OSWECs in the unique conditions of the Caspian Sea. The landscape analysis of available wave data from the region informed the creation of feasible parameter bounds. And the site selection analysis pinpointed a location with strong energy potential based on the optimal wave height and period found by the HC-EGWO. Hence, the outcomes provide a launchpad for harnessing the vast untapped wave resources of the Caspian basin. Looking forward, we emphasize the necessity of integrating field trials into our research to bridge the gap between numerical simulations and real-world applications. These empirical validations will not only corroborate our findings but also refine our optimization algorithms for enhanced efficiency and applicability. Additionally, exploring the environmental impacts and economic viability of wave energy projects will be crucial in promoting sustainable and practical wave energy conversion solutions. Additionally, real-world PTO systems like hydraulic and direct-drive PTOs can be simulated to optimize their parameters. Finally, expanding the optimization to more complex problems like WEC arrays and combining it with control strategy optimization represents promising research directions.

Declaration of Competing Interest

The authors declare that they have no known competing financial interests or personal relationships that could have appeared to influence the work reported in this paper.

Data availability

Data will be made available on request.

Appendix A. Benchmarking the proposed algorithm

In this section, we evaluate the performance of the HC-EGWO algorithm on a total of 16 benchmark functions and analyze the results.

A.1. Benchmark functions

These are classical benchmark functions that have been widely used by researchers in the field. These functions are well-established and are commonly used to evaluate the performance of optimization algorithms.

Table A.7
Multis [92].

Function	Dim	Range	f_{min}
$F_1(x) = \sum_{i=1}^{n}(-x_i \cdot \sin(\sqrt{\lvert x_i \rvert}))$	30	[−500, 500]	−418.9829x5
$F_2(x) = \sum_{i=1}^{n}(x_i^2 - 10 \cdot \cos(2\pi x_i) + 10)$	30	[−5.12, 5.12]	0
$F_3(x) = -20 \cdot \exp\left(-0.2 \cdot \sqrt{\frac{\sum_{i=1}^{n} x_i^2}{n}}\right) - \exp\left(\frac{1}{n}\sum_{i=1}^{n}\cos(2\pi x_i)\right) + 20 + e$	30	[−32, 32]	0
$F_4(x) = \frac{1}{4000}\sum_{i=1}^{n} x_i^2 - \prod_{i=1}^{n}\cos\left(\frac{x_i}{\sqrt{i}}\right) + 1$	30	[−600, 600]	0
$F_5 = \frac{\pi}{n}\left(10\sin(\pi y_1)\right) + \sum_{i=1}^{n-1}(y_i - 1)^2 \cdot \left(1 + 10\sin^2(\pi y_{i+1})\right) + (y_n - 1)^2 + \sum_{i=1}^{n} u(x_i, 10, 100, 4)$ $y_i = 1 + \frac{x_i + 1}{4}$ $u(x_i, a, k, m) =$ $\begin{cases} k(x_i - a)^m & x_i > a \\ 0 & -a < x_i < a \\ k(-x_i - a)^m & x_i < -a \end{cases}$	30	[−100, 100]	0
$F_6(x) = 0.1\left(\sin^2(3\pi x_1) + \sum_{i=1}^{n}\left((x_i - 1)^2 \cdot (1 + \sin^2(3\pi x_i + 1))\right) + (x_n - 1)^2(1 + \sin^2(2\pi x_n))\right) + \sum_{i=1}^{n} U(x_i, 5, 100, 4)$	30	[−50, 50]	0

Table A.8
Fixed-dimension Multimodal Benchmark Functions. [92].

Function	Dim	Range	f_{min}
$F_7 = \left(\frac{1}{500} + \sum_{j=1}^{25}\frac{1}{j + \sum_{i=1}^{2}(x_i - a_{ij})^6}\right)^{-1}$	2	[−65, 65]	1
$F_8(x) = \sum_{i=1}^{11}\left(a_i - \frac{x_1(b_i^2 + x_2 b_i)}{b_i^2 + x_3 b_i + x_4}\right)^2$	4	[−5, 5]	0.00030
$F_9(x) = 4x_1^2 - 2.1x_1^4 + \frac{1}{3}x_1^6 + x_1x_2 - 4x_2^2 + 4x_2^4$	2	[−5, 5]	−1.0316
$F_{10}(x) = \left(x_2 - \frac{5.1}{4\pi^2}x_1^2 + \frac{5}{\pi}x_1 - 6\right)^2 + 10\left(1 - \frac{1}{8\pi}\right)\cos(x_1) + 10$	2	[−5, 5]	0.398
$F_{11}(x) = \left(1 + (x_1 + x_2 + 1)^2(19 - 14x_1 + 3x_1^2 - 14x_2 + 6x_1x_2 + 3x_2^2)\right)\left(30 + (2x_1 - 3x_2)^2(18 - 32x_1 + 12x_1^2 + 48x_2 - 36x_1x_2 + 27x_2^2)\right)$	2	[−2, 2]	3
$F_{12}(x) = -\sum_{i=1}^{4}\left(c_i\exp\left(-\sum_{j=1}^{3}a_{ij}(x_j - p_{ij})^2\right)\right)$	3	[1,3]	−3.86
$F_{13}(x) = -\sum_{i=1}^{4}\left(c_i\exp\left(-\sum_{j=1}^{6}a_{ij}(x_j - p_{ij})^2\right)\right)$	6	[0, 1]	−3.32
$F_{14}(x) = -\sum_{i=1}^{5}\left((X - a_i)(X - a_i)^T + c_i\right)^{-1}$	4	[0, 10]	−10.1532
$F_{15}(x) = -\sum_{i=1}^{7}\left((X - a_i)(X - a_i)^T + c_i\right)^{-1}$	4	[0, 10]	−10.4028
$F_{16}(x) = -\sum_{i=1}^{10}\left((X - a_i)(X - a_i)^T + c_i\right)^{-1}$	4	[0, 10]	10.5363

You can find a detailed list of these classical benchmark functions in Tables A.7 and A.8. The tables provide information such as the dimensionality (Dim) of the function, the range of the function's search space (Range), and the optimal value (fmin) of each function [92]. By benchmarking the HC-EGWO algorithm on these 16 functions, we can evaluate its performance and compare it to other optimization algorithms.

All the benchmark functions employed in this study are aimed at minimizing a given objective. These functions can be classified either as multimodal or fixed-dimension multimodal. To assess the performance of the HC-EGWO, it was executed 30 times on each benchmark function. The results were then analyzed statistically, providing the average and standard deviation values. These statistical outcomes are presented in Tables A.9, which allow for comparing and evaluating the algorithm's performance across the benchmark functions. To validate the results, the HC-EGWO algorithm is compared against the GA and other variations of the GWO algorithm, namely the conventional Grey Wolf Optimizer [92], the modified GWO [93], the Exploration-Enhanced GWO [94], the Improved GWO [96], and the Efficient and Robust GWO [97].

A.2. Benchmark functions results

Based on the results of the landscape analysis, it has been revealed that the problem at hand exhibits a multimodal nature. Therefore, multimodal benchmark functions have been used to test the effectiveness of HC-EGWO to optimize a wide range of complex problems. Furthermore, assessing the performance of HC-EGWO using multimodal benchmark functions can help in clarifying the generalization ability of the optimization method. The importance of generalization lies in its ability to prevent overfitting [109], a situation where an optimization algorithm excessively fine-tunes its parameters to match specific conditions perfectly. Overfitting can result in subpar performance when the algorithm is applied to unfamiliar problem instances. By giving priority to generalization, optimization methods concentrate on capturing fundamental patterns and principles that can be transferred to new problem instances, resulting in solutions that are more dependable and efficient.

These benchmark functions have multiple global and local optima, which increase by the number of dimensions. This characteristic makes them the perfect functions to test the exploration ability of an algorithm [92]. As shown in Table A.9, the HC-EGWO can provide very competitive results (especially in fixed-dimension multimodal benchmark function). This algorithm reaches the best solutions in 7 test functions and the second-best answer in 2 functions in this category, which is the best performance among the analyzed methods. It is notable that in some functions, like F9 and F11, the difference in performance is very minuscule.

Fig. A.21 shows a comparative plot of the five variants of GWO and the proposed GWO (HC-EGWO) performance over the 16 benchmarks. The performance average rank of each variant and the significant differences using the Friedman test can confirm that HC-EGWO performed best in these 16 multi-modal optimization benchmarks. The average

Table A.9
Results of the multimodal benchmark functions.

F	GA	GWO	mGWO	EEGWO	IGWO	ERGWO	HC-EGWO
1 Avg	-2.64E+03	-5.79E+03	-5.35E+03	-2.10E+03	-6.05E+03	-2.20E+03	-5.74E+03
Std	5.08E+02	6.64E+02	1.03E+03	5.00E+02	8.18E+02	4.58E+02	8.15E+02
2 Avg	7.40E+01	3.18E+00	2.84E-14	0.00E+00	7.16E+00	0.00E+00	1.07E+02
Std	1.38E+01	3.61E+00	3.52E-14	0.00E+00	4.39E+00	0.00E+00	2.95E+01
3 Avg	2.31E-03	1.01E-13	2.16E-14	4.44E-16	1.98E-09	4.00E-15	5.18E-14
Std	3.62E-03	1.89E-14	4.25E-15	2.96E-31	1.22E-09	2.37E-30	1.57E-14
4 Avg	4.41E+01	4.78E-03	1.51E-03	0.00E+00	9.00E-03	0.00E+00	1.72E-03
Std	5.14E+00	7.69E-03	4.88E-03	0.00E+00	1.08E-02	0.00E+00	5.59E-03
5 Avg	2.88E+00	3.63E-02	3.84E-02	1.43E+00	7.41E-02	8.41E-01	5.90E-07
Std	1.33E+00	1.57E-02	1.72E-02	1.17E-01	5.16E-02	1.84E-01	3.34E-07
6 Avg	1.29E+01	5.82E-01	5.39E-01	2.99E+00	8.67E-01	2.97E+00	1.32E-02
Std	5.61E+00	2.31E-01	2.03E-01	1.90E-03	2.70E-01	4.83E-02	2.98E-02
7 Avg	5.44E+00	5.49E+00	5.75E+00	1.16E+01	5.63E+00	9.11E+00	4.72E+00
Std	2.33E+00	4.77E+00	4.71E+00	2.72E+00	4.48E+00	3.38E+00	4.04E+00
8 Avg	6.22E-02	5.66E-03	5.66E-03	1.79E-02	3.73E-03	2.82E-03	2.48E-03
Std	4.94E-02	1.20E-02	1.20E-02	1.38E-02	7.44E-03	2.91E-03	5.96E-03
9 Avg	-9.91E-01	-1.03E+00	-1.03E+00	-5.04E-01	-1.03E+00	-1.02E+00	-1.03E+00
Std	4.07E-02	1.61E-08	7.64E-08	2.29E-01	2.83E-12	1.20E-02	5.12E-12
10 Avg	1.05E+00	3.98E-01	3.98E-01	2.55E+00	3.98E-01	7.93E-01	3.98E-01
Std	4.61E-01	5.78E-04	3.93E-05	1.95E+00	7.50E-11	3.37E-01	4.23E-04
11 Avg	3.66E+00	3.00E+00	3.00E+00	6.86E+01	3.00E+00	1.01E+01	3.00E+00
Std	5.28E-01	4.55E-05	2.00E-05	7.02E+01	6.53E-05	1.02E+01	2.34E-05
12 Avg	-3.15E+00	-3.86E+00	-3.86E+00	-3.24E+00	-3.86E+00	-3.42E+00	-3.86E+00
Std	2.38E-02	2.30E-03	2.22E-03	4.69E-01	2.54E-03	3.19E-01	1.90E-03
13 Avg	-2.92E+00	-3.28E+00	-3.28E+00	-1.60E+00	-3.28E+00	-2.00E+00	-3.24E+00
Std	1.78E-01	6.72E-02	6.33E-02	5.85E-01	6.91E-02	4.22E-01	7.68E-02
14 Avg	-1.53E+00	-8.81E+00	-9.40E+00	-7.85E-01	-9.64E+00	-2.46E+00	-9.21E+00
Std	3.00E-01	2.50E+00	1.92E+00	1.91E-01	1.53E+00	5.77E-01	2.15E+00
15 Avg	-1.54E+00	-1.02E+01	-1.02E+01	-8.12E-01	-1.02E+01	-2.38E+00	-1.00E+01
Std	3.55E-01	9.54E-01	9.53E-01	2.07E-01	9.54E-01	7.80E-01	1.32E+00
16 Avg	-1.62E+00	-9.81E+00	-1.01E+01	-9.01E-01	-9.79E+00	-2.47E+00	-1.05E+01
Std	7.77E-01	2.20E+00	1.72E+00	2.40E-01	2.29E+00	5.54E-01	6.47E-08

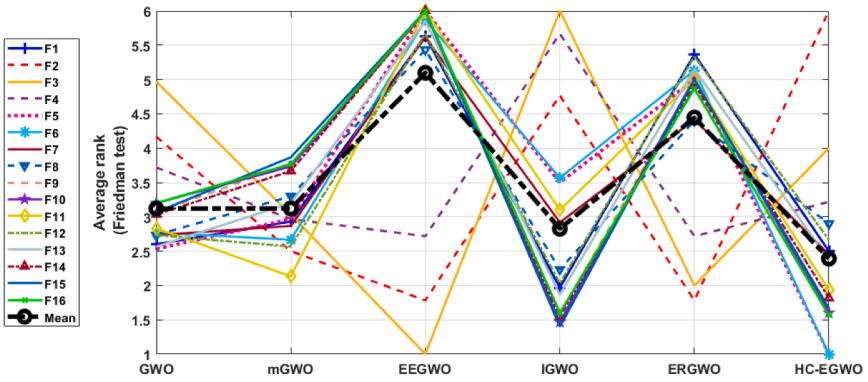

Fig. A.21. Average performance rank of the HC-EGWO compared with other five variants of GWOs over the 16 benchmarks using the Friedman test.

rank is used to calculate the Friedman statistic, which is compared to the critical value to determine whether there are significant differences in performance.

References

[1] Melikoglu Mehmet. Current status and future of ocean energy sources: a global review. Ocean Eng 2018;148:563–73.
[2] González-Ramírez Xiomara, Guzmán-Cabrera Rafael, Hernández-Robles Iván A, Guzmán-Sepúlveda José R. Statistical technique to improve the wave potential

estimation for the design of wave electric generators. Energy Convers Manage: X 2022;14:100220.
[3] Hu Huakun, Xue Wendong, Jiang Peng, Li Yong. Bibliometric analysis for ocean renewable energy: an comprehensive review for hotspots, frontiers, and emerging trends. Renew Sustain Energy Rev 2022;167:112739.
[4] Chen Weixing, Lin Xiongsen, Lu Yunfei, Li Shaoxun, Wang Lucai, Zhang Yongkuang, et al. Design and experiment of a double-wing wave energy converter. Renew Energy 2023;202:1497–506.
[5] Amini Erfan, Mehdipour Hossein, Faraggiana Emilio, Golbaz Danial, Mozaffari Sevda, Bracco Giovanni, et al. Optimization of hydraulic power take-off system settings for point absorber wave energy converter. Renew Energy 2022; 194:938–54.
[6] Golbaz Danial, Asadi Rojin, Amini Erfan, Mehdipour Hossein, Nasiri Mahdieh, Etaati Bahareh, et al.. Layout and design optimization of ocean wave energy converters: a scoping review of state-of-the-art canonical, hybrid, cooperative, and combinatorial optimization methods. Energy Rep 2022;8:15446–15479.
[7] Rosati M, Henriques JCC, Ringwood JV. Oscillating-water-column wave energy converters: a critical review of numerical modelling and control. Energy Convers Manage: X, page 100322, 2022.
[8] Carrelhas AAD, Gato LMC, Henriques JCC, Marques GD. Estimation of generator electrical power output and turbine torque in modelling and field testing of owc wave energy converters. Energy Convers Manage: X 2023;19:100384.
[9] Drew Benjamin, Plummer Andrew R, Necip Sahinkaya M. A review of wave energy converter technology; 2009.
[10] Abazari A, Aziminia MM. Enhanced power extraction by splitting a single flap-type wave energy converter into a double configuration. Renew Energy Res Appl 2022.
[11] Ahmed Ammar, Azam Ali, Wang Yanen, Tan Xing, Yi Minyi, Zhang Zutao. On the s-shaped floaters for a wavestar-like wave energy converter with an i-shaped mechanical power take-off. Energy Convers Manage: X 2023;19:100387.
[12] Zhai Qiang, Li Tong, Liu Yizhi. Life cycle assessment of a wave energy converter: uncertainties and sensitivities. J Clean Prod 2021;298:126719.
[13] Chen Shao-En, Chen Wan-Yi, Yang Ray-Yeng, Wu Chia-Che. A piezoelectric wave energy harvester equipped with a sequential-drive rotating mechanism and rotary piezoelectric harvesting component. Energy Convers Manage: X 2023;20:100463.
[14] Cheng Yong, Tang Lianyang, Ji Chunyan. Three-dimensional hydrodynamic analysis and efficiency optimization of submerged multi-cylindrical oscillating wave surge converter. Ocean Eng. 2020;215:107710.
[15] Ghasemipour Nima, Izanlou Pouria, Jahangir Mohammad Hossein. Feasibility study on utilizing oscillating wave surge converters (owscs) in nearshore regions, case study: along the southeastern coast of iran in oman sea. J Clean Prod 2022; 367:133090.
[16] Folley Matthew, Whittaker TJT, Henry Alan. The effect of water depth on the performance of a small surging wave energy converter. Ocean Eng 2007;34(8–9): 1265–74.
[17] Folley Matthew, Whittaker Trevor, Van't Hoff J. The design of small seabed-mounted bottom-hinged wave energy converters. In: Proceedings of the 7th European wave and tidal energy conference. Citeseer, vol. 455; 2007. p. 312.
[18] Renzi Emiliano, Dias Frederic. Hydrodynamics of the oscillating wave surge converter in the open ocean. Eur J Mech-B/Fluids 2013;41:1–10.
[19] Porter R, Biggs NRT. Wave energy absorption by a flap-type oscillating wave surge converter. University of Bristol-Department of Mathematics-Study. Available online: http://www.maths.bris.ac.uk/marp/publications.html (accessed on 6 April 2016), 2012.
[20] Choiniere Michael A, Tom Nathan M, Thiagarajan Krish P. Load shedding characteristics of an oscillating surge wave energy converter with variable geometry. Ocean Eng 2019;186:105982.
[21] Liu Zhenqing, Wang Yize, Hua Xugang. Numerical studies and proposal of design equations on cylindrical oscillating wave surge converters under regular waves using sph. Energy Convers Manage 2020;203:112242.
[22] Gomes RPF, Lopes MFP, Henriques JCC, Gato LMC, Falcao AFO. The dynamics and power extraction of bottom-hinged plate wave energy converters in regular and irregular waves. Ocean Eng 2015;96:86–99.
[23] Qiu Shou-qiang, Ye Jia-wei, Wang Dong-jiao, Liang Fu-lin. Experimental study on a pendulum wave energy converter. China Ocean Eng 2013;27(3):359–68.
[24] Lin Chen-Chou, Chow Yi-Chih, Tzang Shiaw-Yih. The viscous effect in power capture of bottom–hinged oscillating wave surge converters. In Proceedings of the 4rd Asian Wave and Tidal Energy Conference (AWTEC), Taipei, Taiwan, pages 423–1.
[25] Mérigaud Alexis, Ringwood John V. A nonlinear frequency-domain approach for numerical simulation of wave energy converters. IEEE Trans Sustain Energy 2017;9(1):86–94.
[26] Yu Yi-Hsiang, Li Ye. Reynolds-averaged navier–stokes simulation of the heave performance of a two-body floating-point absorber wave energy system. Comput Fluids 2013;73:104–14.
[27] Schmitt Pál, Asmuth Henrik, Elsäßer Björn. Optimising power take-off of an oscillating wave surge converter using high fidelity numerical simulations. Int J Mar Energy 2016;16:196–208.
[28] Davidson Josh, Costello Ronan. Efficient nonlinear hydrodynamic models for wave energy converter design—a scoping study. J Mar Sci Eng 2020;8(1):35.
[29] Davidson Josh, Karimov Mirlan, Szelechman Adam, Windt Christian, Ringwood J. Dynamic mesh motion in openfoam for wave energy converter simulation. In 14th OpenFOAM Workshop; 2019.
[30] Katsidoniotaki Eirini, Göteman Malin. Numerical modeling of extreme wave interaction with point-absorber using openfoam. Ocean Eng 2022;245:110268.
[31] Chen Weixing, Wu Zheng, Liu Jimu, Jin Zhenlin, Zhang Xiantao, Gao Feng. Efficiency analysis of a 3-dof wave energy converter (sjtu-wec) based on modeling, simulation and experiment. Energy 2021;220:119718.
[32] Lawson Michael, Yu Yi-Hsiang, Ruehl Kelley, Michelen Carlos, et al. Development and demonstration of the wec-sim wave energy converter simulation tool; 2014.
[33] Yu Yi-Hsiang, Keester Adam, Tom Nathan, Forbush Dominic, Leon Jorge, Grasberger Jeff, et al.. Wec-sim v5.0.1; 2022.
[34] Tan Jian, Polinder Henk, Laguna Antonio Jarquin, Miedema Sape. A wave-to-wire analysis of the adjustable draft point absorber wave energy converter coupled with a linear permanent-magnet generator. Ocean Eng 2023;276:114195.
[35] Burge Cole, Tom Nathan, Thiagarajan Krish, Davis Jacob, Nguyen Nhu. Performance modeling of a variable-geometry oscillating surge wave energy converter on a raised foundation. In: International Conference on Offshore Mechanics and Arctic Engineering, vol. 85192. American Society of Mechanical Engineers; 2021. page V009T09A010.
[36] Husain Salman, Davis Jacob, Tom Nathan, Thiagarajan Krish, Burge Cole, Nguyen Nhu. Influence on structural loading of a wave energy converter by controlling variable-geometry components and the power take-off. In: International Conference on Offshore Mechanics and Arctic Engineering, vol. 85932. American Society of Mechanical Engineers; 2022. page V008T09A087. ssss.
[37] Amini Erfan. Locating, designing and evaluating the Oscillating Surge Wave Energy Converter using Grey Wolf Optimizer algorithm [Ph.D. thesis]. University of Tehran; 2019.
[38] Bosma Bret, Simmons Asher, Lomonaco Pedro, Ruehl Kelley, Gunawan Budi. wec-sim phase 1 validation testing: experimental setup and initial results. In: International Conference on Offshore Mechanics and Arctic Engineering, vol. 49972. American Society of Mechanical Engineers; 2016. page V006T09A025.
[39] Ruehl Kelley, Michelen Carlos, Bosma Bret, Yu Yi-Hsiang. Wec-sim phase 1 validation testing: numerical modeling of experiments. In: International Conference on Offshore Mechanics and Arctic Engineering, vol. 49972. American Society of Mechanical Engineers; 2016. page V006T09A026.
[40] Mi Jia, Huang Jianuo, Li Xiaofan, Yang Lisheng, Ahmed Alaa, Datla Raju, Folly Matt, Hajj Muhammad, Zuo Lei. Dual-flap floating oscillating surge wave energy converter: modelling and experiment evaluation. IFAC-PapersOnLine 2022;55(27):138–43.
[41] Sricharan VVS, Chandrasekaran Srinivasan. Time-domain analysis of a bean-shaped multi-body floating wave energy converter with a hydraulic power take-off using wec-sim. Energy 2021;223:119985.
[42] Choiniere Michael A, Thiagarajan Krish, Tom Nathan M. Study of a novel oscillating surge wave energy converter. In: Proceedings of Offshore Energy and Storage; 2017. p. 1–11 (1).
[43] Shadmani Alireza, Nikoo Mohammad Reza, Gandomi Amir H. Robust optimization of pto settings for point absorber wave energy converter. In: In: Kulkarni, A.J., Gandomi, A.H. (eds) Handbook of Formal Optimization. Springer, Singapore;; 2023. p. 1–19.
[44] Sheng Wanan, Lewis Anthony. Power takeoff optimization for maximizing energy conversion of wave-activated bodies. IEEE J Oceanic Eng 2016;41(3):529–40.
[45] Sheng Wanan, Lewis Anthony. Power takeoff optimization to maximize wave energy conversions for oscillating water column devices. IEEE J Oceanic Eng 2017;43(1):36–47.
[46] Zhang Dahai, Huang Haocai, Chen Ying, Zhao Haitao, Li Wei. State-dependent model of a hydraulic power takeoff for an inverse pendulum wave energy converter. Mar Technol Soc J 2015;49(5):38–48.
[47] Zhang Wei. Parameter adjustment strategy and experimental development of hydraulic system for wave energy power generation. Symmetry 2020;12(5):711.
[48] Rezaei Saeed, Rahimi Amir, Parvizian Jamshid, Mansoorzadeh Shahriar. Experimental and numerical study of a novel unidirectional mechanical power take-off system for two-body wave energy converters. Energy Convers Manage: X 2023;19:100385.
[49] Fang Hong-Wei, Feng Yu-Zhu, Li Guo-Ping. Optimization of wave energy converter arrays by an improved differential evolution algorithm. Energies 2018; 11(12):3522.
[50] Gomes RPF, Henriques JCC, Gato LMC, de O Falcão AF. Hydrodynamic optimization of an axisymmetric floating oscillating water column for wave energy conversion. Renew Energy 2012;44:328–39.
[51] Esmaeilzadeh Soheil, Alam Mohammad-Reza. Shape optimization of wave energy converters for broadband directional incident waves. Ocean Eng 2019;174: 186–200.
[52] Lyu Jianyang, Abdelkhalik Ossama, Gauchia Lucia. Optimization of dimensions and layout of an array of wave energy converters. Ocean Eng. 2019;192:106543.
[53] Shadmani Alireza, Nikoo Mohammad Reza, Etri Talal, Gandomi Amir H. A multi-objective approach for location and layout optimization of wave energy converters. Appl Energy 2023;347:121397.
[54] Garcia-Teruel Anna, DuPont Bryony, Forehand David IM. Hull geometry optimisation of wave energy converters: on the choice of the optimisation algorithm and the geometry definition. Appl Energy 2020;280:115952.
[55] Liu Chunyuan, Chen Yi, Dong Rui, Ye Baolin. Optimization design of tubular permanent magnet linear generator based on entropy model for wave energy conversion. Available at SSRN 4312827.
[56] Aubry Judicaël, Ahmed Hamid Ben, Multon Bernard. Sizing optimization methodology of a surface permanent magnet machine-converter system over a torque-speed operating profile: application to a wave energy converter. IEEE Trans Industr Electron 2011;59(5):2116–25.
[57] Neshat Mehdi, Sergiienko Nataliia Y, Mirjalili Seyedali, Nezhad Meysam Majidi, Piras Giuseppe, Garcia Davide Astiaso. Multi-mode wave energy converter design

optimisation using an improved moth flame optimisation algorithm. Energies 2021;14(13):3737.
[58] Das Tapas K, Kerikous Emeel, Venkatesan Nithya, Janiga Gabor, Thévenin Dominique, Samad Abdus. Performance improvement of a wells turbine through an automated optimization technique. Energy Convers Manage: X 2022; 16:100285.
[59] Amini Erfan, Nasiri Mahdieh, Pargoo Navid Salami, Mozhgani Zahra, Golbaz Danial, Baniesmaeil Mehrdad, et al. Design optimization of ocean renewable energy converter using a combined bi-level metaheuristic approach. Energy Convers Manage: X 2023;19:100371.
[60] Zhang Nan, Feng Chen, Shan Yahui, Sun Na, Xue Xiaoming, Shi Liping. A universal stability quantification method for grid-connected hydropower plant considering fopi controller and complex nonlinear characteristics based on improved gwo. Renew Energy 2023;211:874–94.
[61] Sayed Enas Taha, Olabi AG, Elsaid Khaled, Al Radi Muaz, Semeraro Concetta, Doranehgard Mohammad Hossein, et al. Application of artificial intelligence techniques for modeling, optimizing, and controlling desalination systems powered by renewable energy resources. J Clean Prod 2023;413:137486.
[62] Shadmani Alireza, Nikoo Mohammad Reza, Gandomi Amir H, Wang Ruo-Qian, Golparvar Behzad. A review of machine learning and deep learning applications in wave energy forecasting and wec optimization. Energy Strategy Rev 2023;49: 101180.
[63] Neshat Mehdi, Alexander Bradley, Sergiienko Nataliia Y, Wagner Markus. New insights into position optimisation of wave energy converters using hybrid local search. Swarm Evol Comput 2020;59:100744.
[64] Neshat Mehdi, Alexander Bradley, Sergiienko Nataliia Y, Wagner Markus. Optimisation of large wave farms using a multi-strategy evolutionary framework. In: Proceedings of the 2020 genetic and evolutionary computation conference; 2020. p. 1150–8.
[65] Amini Erfan, Mehdipour Hossein, Faraggiana Emilio, Golbaz Danial, Mozaffari Sevda, Bracco Giovanni, et al. Optimization study of hydraulic power take-off system for an ocean wave energy converter. arXiv preprint arXiv:2112.09803; 2021.
[66] Kamranzad Bahareh, Etemad-Shahidi Amir, Chegini Vahid. Sustainability of wave energy resources in southern caspian sea. Energy 2016;97:549–59.
[67] Alamian Rezvan, Shafaghat Rouzbeh, Jalal Miri S, Yazdanshenas Nima, Shakeri Mostafa. Evaluation of technologies for harvesting wave energy in caspian sea. Renew Sustain Energy Rev 2014;32:468–476.
[68] Amirinia Gholamreza, Kamranzad Bahareh, Mafi Somayeh. Wind and wave energy potential in southern caspian sea using uncertainty analysis. Energy 2017; 120:332–45.
[69] Alamian Rezvan, Shafaghat Rouzbeh, Hosseini Seyed Saeed, Zainali Amir. Wave energy potential along the southern coast of the caspian sea. Int J Mar Energy 2017;19:221–34.
[70] Amini Erfan, Asadi Rojin, Golbaz Danial, Nasiri Mahdieh, Naeeni Seyed Taghi Omid, Nezhad Meysam Majidi, et al. Comparative study of oscillating surge wave energy converter performance: A case study for southern coasts of the caspian sea. Sustainability 2021;13(19):10932.
[71] Hossein Jahangir Mohammad, Mazinani Mehran. Evaluation of the convertible offshore wave energy capacity of the southern strip of the caspian sea. Renew Energy 2020;152:331–46.
[72] Aghanezhad M, Shafaghat R, Alamian R, Seyedi SMA, Raji Asadabadi MJ. Experimental study on performance assessment of hydraulic power take-off system in centipede wave energy converter considering caspian sea wave characteristics. Int J Eng 2022;35(5):883–99.
[73] Iuppa C, Cavallaro L, Vicinanza Diego, Foti Enrico. Investigation of suitable sites for wave energy converters around sicily (italy). Ocean Sci 2015;11(4):543–57.
[74] Galparsoro Ibon, Liria Pedro, Legorburu Irati, Bald Juan, Chust Guillem, Ruiz-Minguela Pablo, Pérez Germán, Marqués Javier, Torre-Enciso Yago, González Manuel, et al. A marine spatial planning approach to select suitable areas for installing wave energy converters (wecs), on the basque continental shelf (bay of biscay). Coastal Manage 2012;40(1):1–19.
[75] Ergul Engin Ufuk, Ozbek Tayfun. Wave-energy plant site and converter type selection using multi-criteria decision making. Proc Inst Civil Eng-Energy 2022; 175(2):49–63.
[76] Kamranzad Bahareh, Hadadpour Sanaz. A multi-criteria approach for selection of wave energy converter/location. Energy 2020;204:117924.
[77] Kamranzad Bahareh, Lin Pengzhi, Iglesias Gregorio. Combining methodologies on the impact of inter and intra-annual variation of wave energy on selection of suitable location and technology. Renew Energy 2021;172:697–713.
[78] Carballo R, Sánchez M, Ramos V, Castro A. A tool for combined wec-site selection throughout a coastal region: Rias baixas, nw spain. Appl Energy 2014;135:11–9.
[79] Xu Xinxin, Robertson Bryson, Buckham Bradley. A techno-economic approach to wave energy resource assessment and development site identification. Appl Energy 2020;260:114317.
[80] Wang Chia-Nan, Nhieu Nhat-Luong, Nguyen Hoang-Phu, Wang Jing-Wein. Simulation-based optimization integrated multiple criteria decision-making framework for wave energy site selection: a case study of australia. IEEE Access 2021;9:167458–76.
[81] Dyakonov Gleb S, Ibrayev Rashit A. Long-term evolution of caspian sea thermohaline properties reconstructed in an eddy-resolving ocean general circulation model. Ocean Sci 2019;15(3):527–41.
[82] Taebi S, Golshani A. Long term characteristics of waves in the caspian sea, the persian gulf and the gulf of oman. COPEDEC VII 2008.
[83] Van't Hoff Joseph. Hydrodynamic modelling of the oscillating wave surge converter [Ph.D. thesis]. Queen's University Belfast; 2009.
[84] Gomes R, Lopes M, Henriques JCC, Gato LMC, Falcão AFO. A study on the wave energy conversion by submerged bottom-hinged plates. In: 9th European Wave and Tidal Energy Conference, Southampton, UK; 2011.
[85] Senol Koray, Raessi Mehdi. Enhancing power extraction in bottom-hinged flap-type wave energy converters through advanced power take-off techniques. Ocean Eng 2019;182:248–58.
[86] Han Shifen, Xiao Li. An improved adaptive genetic algorithm. In SHS Web of Conferences, volume 140, page 01044. EDP Sciences; 2022.
[87] Wang Dongshu, Tan Dapei, Liu Lei. Particle swarm optimization algorithm: an overview. Soft Comput 2018;22:387–408.
[88] Yin Ershuai, Li Qiang. Device performance matching and optimization of photovoltaic-thermoelectric hybrid system. Energy Convers Manage: X 2021;12: 100115.
[89] Ennemiri Naoufel, Berrada Asmae, Emrani Anisa, Abdelmajid Jamil, El Mrabet Rachid. Optimization of an off-grid pv/biogas/battery hybrid energy system for electrification: A case study in a commercial platform in morocco. Energy Convers Manage: X 2024;21:100508.
[90] Saadaoui Driss, Elyaqouti Mustapha, Assalaou Khalid, Lidaighbi Souad, et al. Parameters optimization of solar pv cell/module using genetic algorithm based on non-uniform mutation. Energy Convers Manage: X 2021;12:100129.
[91] Abdollahzadeh Benyamin, Gharehchopogh Farhad Soleimanian, Mirjalili Seyedali. Artificial gorilla troops optimizer: a new nature-inspired metaheuristic algorithm for global optimization problems. Int J Intell Syst 2021; 36(10):5887–958.
[92] Mirjalili Seyedali, Mirjalili Seyed Mohammad, Lewis Andrew. Grey wolf optimizer. Adv Eng Software 2014;69:46–61.
[93] Mittal Nitin, Singh Urvinder, Sohi Balwinder Singh. Modified grey wolf optimizer for global engineering optimization. Applied Computational Intelligence and Soft Computing, 2016 2016.
[94] Long Wen, Jiao Jianjun, Liang Ximing, Tang Mingzhu. An exploration-enhanced grey wolf optimizer to solve high-dimensional numerical optimization. Eng Appl Artif Intell 2018;68:63–80.
[95] Zafar Muhammad Hamza, Khan Noman Mujeeb, Mirza Adeel Feroz, Mansoor Majad. Bio-inspired optimization algorithms based maximum power point tracking technique for photovoltaic systems under partial shading and complex partial shading conditions. J Clean Prod 2021;309:127279.
[96] Ma Xiang, Duan Jiandong, Wang Xiao, Song Tuo, Wang Yanhang, Song Ting. Research of photovoltaic systems mppt based on improved grey wolf algorithm under partial shading conditions. In 2018 2nd IEEE Conference on Energy Internet and Energy System Integration (EI2), pages 1–6. IEEE, 2018.
[97] Long Wen, Cai Shaohong, Jiao Jianjun, Tang Mingzhu. An efficient and robust grey wolf optimizer algorithm for large-scale numerical optimization. Soft. Comput. 2020;24(2):997–1026.
[98] Meng Anbo, Zeng Cong, Wang Peng, Chen De, Zhou Tianmin, Zheng Xiaoying, Yin Hao. A high-performance crisscross search based grey wolf optimizer for solving optimal power flow problem. Energy 2021;225:120211.
[99] Sharp Chris, DuPont Bryony. Wave energy converter array optimization: a review of current work and preliminary results of a genetic algorithm approach introducing cost factors. In: International Design Engineering Technical Conferences and Computers and Information in Engineering Conference, vol. 57076. American Society of Mechanical Engineers; 2015. page V02AT03A025.
[100] Giassi Marianna, Göteman Malin. Parameter optimization in wave energy design by a genetic algorithm. In 32nd International Workshop on Water Waves and Floating Bodies (IWWWFB), 23–26th April, 2017, Dalian, China., 2017.
[101] Zeng Xiaohui, Wang Qi, Kang Yuanshun, Yu Fajun. Hydrodynamic interactions among wave energy converter array and a hierarchical genetic algorithm for layout optimization. Ocean Eng 2022;256:111521.
[102] Abdelkhalik Ossama, Darani Shadi. Optimization of nonlinear wave energy converters. Ocean Eng 2018;162:187–95.
[103] Sharp Chris, DuPont Bryony. A multi-objective real-coded genetic algorithm method for wave energy converter array optimization. In: International Conference on Offshore Mechanics and Arctic Engineering, vol. 49972. American Society of Mechanical Engineers; 2016. page V006T09A027.
[104] Quartier Nicolas. Numerical implementation of the power-take-off (pto) of two types of generic wave energy converters using wec-sim. Ghent University; 2018.
[105] Brodersen Katie M, Bywater Emily A, Lanter Alec M, Schennum Hayden H, Furia Kumansh N, Sheth Maulee K, et al. Direct-drive ocean wave-powered batch reverse osmosis. Desalination 2022;523:115393.
[106] Taheri Abdolrahim, Siahtiri Reza. Steel catenary riser-seabed interaction due to caspian sea environmental conditions. J Rehab Civil Eng 2017;5(2):36–48.
[107] Akbarizadeh Naghmeh, Javad Ketabdari Mohammad. Comparative study of tlp and etlp performance in caspian sea environment using numerical method. Mar Struct 2022;86:103279.
[108] Saltelli Andrea, Aleksankina Ksenia, Becker William, Fennell Pamela, Ferretti Federico, Holst Niels, Li Sushan, Wu Qiongli. Why so many published sensitivity analyses are false: a systematic review of sensitivity analysis practices. Environ Model Software 2019;114:29–39.
[109] Han Honggui, Wu Xiaolong, Liu Hongxu, Qiao Junfei. An efficient optimization method for improving generalization performance of fuzzy neural networks. IEEE Trans Fuzzy Syst 2018;27(7):1347–61.